2.2. THE RESULTS OF THE CURRENT FLIGHT SCIENTIFIC PROGRAMMES OF INVESTIGATION AND OBSERVATION

2.2.1. Space Research Institute of the RAS

2.2.1.1. Solar system exploration

1. MARS

1.1. Seasonal distribution of ozone and the O_2 emission. Global climatology of ozone from SPICAM measurements

The SPICAM spectrometer onboard Mars-Express started to observe the red planet in January 2004. The spectrometer allows realizing three methods of ozone observations at once. At nadir the simultaneous observations of integrated ozone abundance in the column of the atmosphere are performed using the Hartley band (220–280 nm) in UV channel (118–320 nm, resolution ~0.51 nm) and the measurement of the $O_2\,^1\Delta_g$ emission in IR channel from 1.27 μm. The emission is a result of the ozone photodissociation and it is more sensitive to ozone abundance which is higher 20 km. In the solar and stellar occultation mode the spectrometer allows to perform measurements of vertical distribution of ozone from the Hartley band in UV at the altitude from 20 to 70 km.

For the first Martian year of observations from January 2004 to Mars 2006 the seasonal distributions of ozone abundance in the column and the $O_2\,^1\Delta_g$ emission have been obtained for the first time of 30th history of Mars exploration.

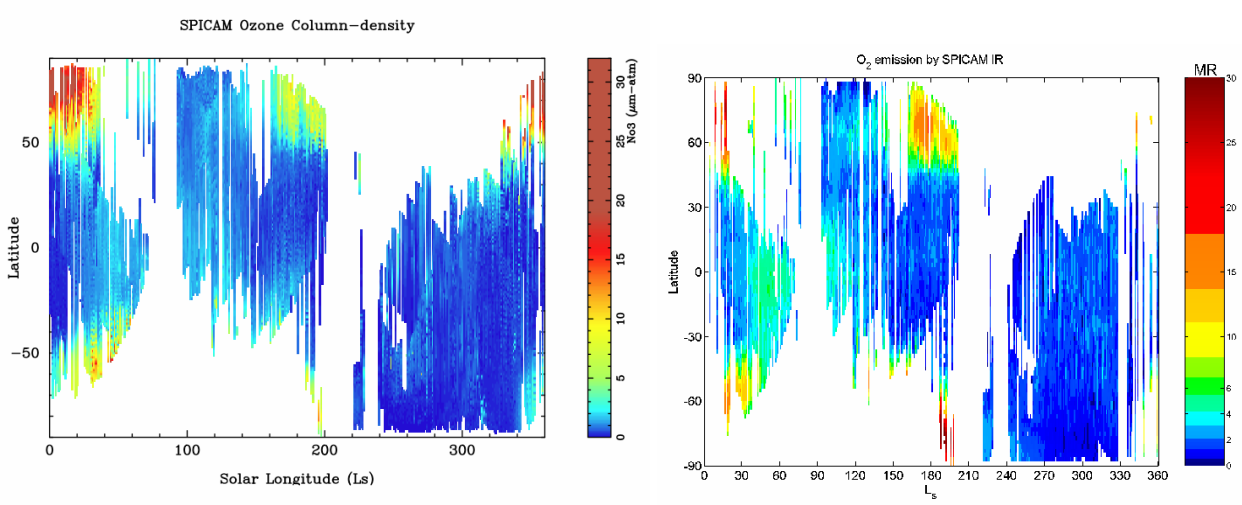

Main results:

- large increases in the ozone column density at high latitudes during late winter-early spring of each hemisphere that totally disappear during summer;

- a large variability of the northern spring content related to the polar vortex oscillations;
- low ozone columns in the equatorial regions all year long;

At low latitudes (3° S–3° N) the seasonal evolution of the O2 emission shows a distinct maximum (5–7 MR) near aphelion. It could be related to seasonal variations of water vapor saturation altitude which controls the ozone distribution in the Martian atmosphere.

1.2. Detection of CO_2 ice clouds in Mars mesosphere with stellar occultation SPICAM/Mars Express measurements

The formation of CO_2 ice clouds in the upper atmosphere of Mars has been suggested in the past on the basis of a few temperature profiles exhibiting portions colder than CO_2 frost point. However, the corresponding clouds were never observed. In this paper, we discuss the detection of the highest clouds ever observed on Mars by the SPICAM ultraviolet spectrometer on board Mars Express spacecraft. Analyzing stellar occultations, several mesospheric detached layers at about 100 km in the southern winter subtropical latitudes were detected, revealing that clouds formed where simultaneous temperature measurements indicated that CO_2 was highly supersaturated and probably condensing. Further analysis of the spectra reveals a cloud opacity in the subvisible range and ice crystals smaller than 100 nm in radius. These layers are therefore similar in nature as the noctilucent clouds which appear on Earth in the polar mesosphere. We interpret these phenomena as CO_2 ice clouds forming inside supersaturated pockets of air created by upward propagating thermal waves. This detection of clouds in such an ultrararefied and supercold atmosphere raises important questions about the martian middle-atmosphere dynamics and microphysics. In particular, the presence of condensates at such high altitudes begs the question of the origin of the condensation nuclei.

1.3. Vertical profiles of aerosol and detection of submicron-sized particles in the Martian atmosphere by UV limb and occultation measurements

Observations made by the SPICAM ultraviolet spectrometer on board the Mars Express orbiter provided several hundreds of atmospheric profiles which have been collected over 3/4 of a Martian year by making use of the stellar occultation and limb observation techniques. The typical structure of the Martian haze possesses at least one discrete layer (60 % of all cases) standing over an extended portion where the opacity continuously increases down to the surface. Differences of morphology are noted between profiles observed near the equator and profiles collected elsewhere. The Martian haze exhibits a pronounced seasonal signal manifested by variations of the maximum elevation at which particles are observed. For reasons related to both convective activity and changes in the hygropause level, cold regions display a much lower haze top than warm regions. Using UV spectrometry

data, we put constraints on haze microphysical properties. Vertical variations of particle size are correlated to variations of opacity; e.g., an increase of particle size is systematically observed near extinction peaks, pointing out cloud formation.. The optical depth of detached cloud layers lofted above 40 km ranges between 0.01 and 0.1 in the visible. Estimation of cloud particle size generally yields a minimum radius value of about 0.3 mm, while several estimates are consistent with a robust 0.1–0.2 mm. Despite marked differences of aerosol profiles between low and high latitudes, haze properties above 60 km remain invariant, possibly reflecting the long-term presence of a background submicronic particle population. Observations made in the southern winter polar night indicate a very clean atmosphere $\tau < 0.1$, with aerosol confined to lower heights and made of particles having a radius on the order of 0.1 mm.

Several profiles of light scattered at the limb of Mars obtained by SPICAM UV revealed that both cloud particles and dust particles above 20 km are in the range 10 to 100 nm. Such particles are much smaller than micron-sized dust particles previously observed in the lower atmosphere, generally from landers.

1.4. Water vapor in the Martian atmosphere by SPICAM IR/Mars-Express: two years of observations

The near-IR channel of SPICAM experiment on Mars Express spacecraft is a 800g acousto-optic tunable filter (AOTF)-based spectrometer operating in the spectral range of 1–1.7 μm with resolving power of ~2000. The nadir measurements of H_2O in the 1.37-μm spectral band are one of the main objectives of the experiment. Three spectrometers on Mars-Express perform simultaneously measurements of water vapor abundance on Mars. SPICAM has shown a low value of H_2O compared to other experiments. As a result the spare model of SPICAM IR instrument was recalibrated in June 2007 in Reims, to analyze specifically the sensitivity to the H_2O vapor band. The obtained calibration has been used for the new analysis of SPICAM IR water vapour measurements. Moreover, as compared with previous analysis, the spectroscopic database HITRAN2004 instead of HITRAN 2000 and the most recent measurements of the water line-width broadening in CO_2 atmosphere have been used. We present the results from January 2004 ($L_S = 330°$, MY26) to August 2007 ($L_S = 287°$, MY28), i.e. almost two Martian years. The seasonal trend of water vapor obtained by SPICAM IR for MY27 is consistent with TES results and disagrees with MAWD South pole maximum measurements. The maximum abundance is 50–55 pr. μm at the North Pole (during MY28 data are missing) and 13-16 pr.μm at the south pole. The northern tropical maximum amounts to 12–15 pr μm. The South Pole maximum for MY28 ($L_S = 260–300$) agrees well with the MAWD South Pole measurements in 1977 and disagrees with the southern maximum of MY27. It assumes the same dust conditions and global dust storm happened at L_S 270 like during the MAWD observations due to the sensitivity of 1.37-μm band depth to aerosol scattering during the dust storm. The maximum near 30-60S at $L_S = 260$ relates to Hellas observations.

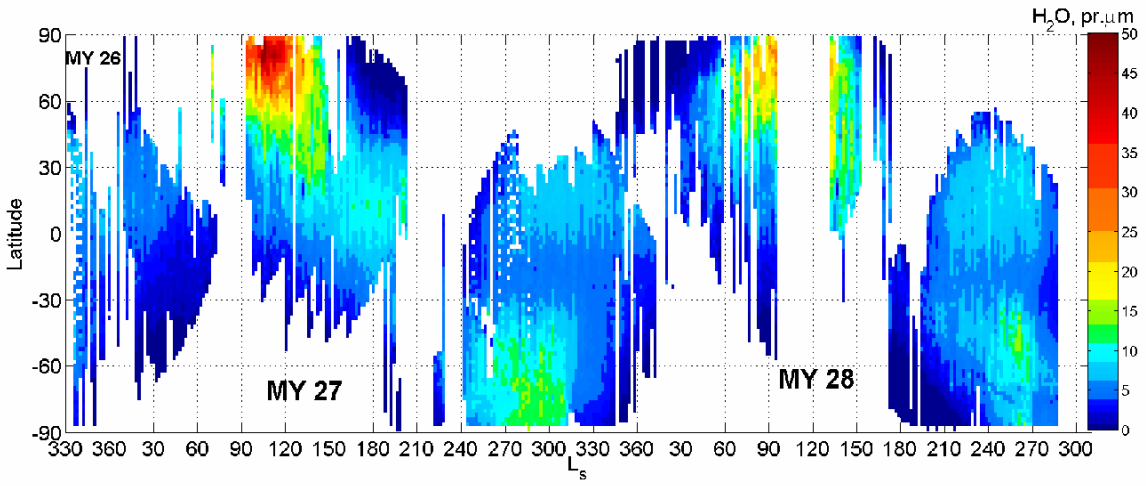

1.5. Study of the Martian water cycle by the PFS and OMEGA experiments onboard the Mars Express

Water vapour is the most variable trace gas in the atmosphere of Mars. This implies that the gas is strongly involved in exchange with non-atmospheric reservoirs on the planet like polar caps, regolith, and possibly permafrost. One of the main goals of the Mars Express mission is to study the Martian water cycle. This work focused on the analysis of observations made by Planetary Fourier Spectrometer (PFS) and the infrared mapping spectrometer OMEGA. The main results are investigation of the seasonal cycle of atmospheric water and the peculiarities related to the Tharsis volcanoes.

Seasonal water cycle

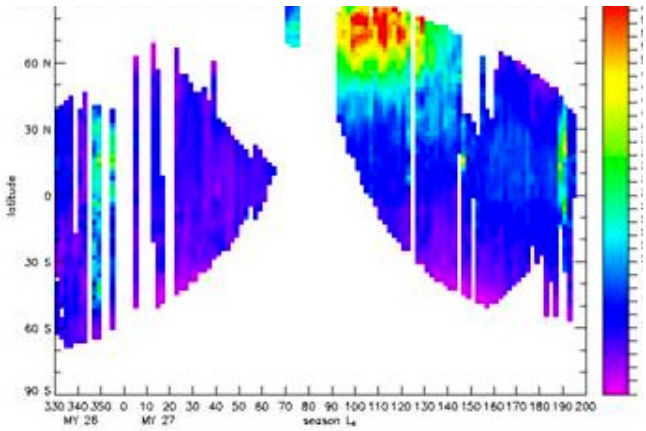

Figure 1: The seasonal map of water vapour between L_s = 330° (MY26) and L_S = 200° (MY27).

Retrievals of the atmospheric water amount was based on the fitting of the PFS spectrum in the region of the 2.56 μm H2O band. The processed dataset includes the time from January 2004 to April 2005 that corresponds to the season between

$L_S = 331°$ (MY26) and $L_S = 196°$ (MY27). Figure 1 shows the seasonal behaviour of the atmospheric water content. The mean column density of the equinox season before northern summer is 8.2 pr.µm. The maximum reached values during northern summer ($L_S = 110°$) are 65 pr.µm, centered around 75 N latitude. After $L_S = 130°$ the maximum vanishes quickly within ~50 days. Manifestation of the equatorward water transport is seen as a "tongue" of 15–20 pr.µm that progressed southward and reached the equator at about $L_S = 190°$ (Fig. 1). The geographical distribution shows two maxima over Arabia Terra and the Tharsis highlands which are most probably caused by atmosphere-ground interaction and by atmospheric circulation.

Water vapour anomaly above Tharsis volcanoes

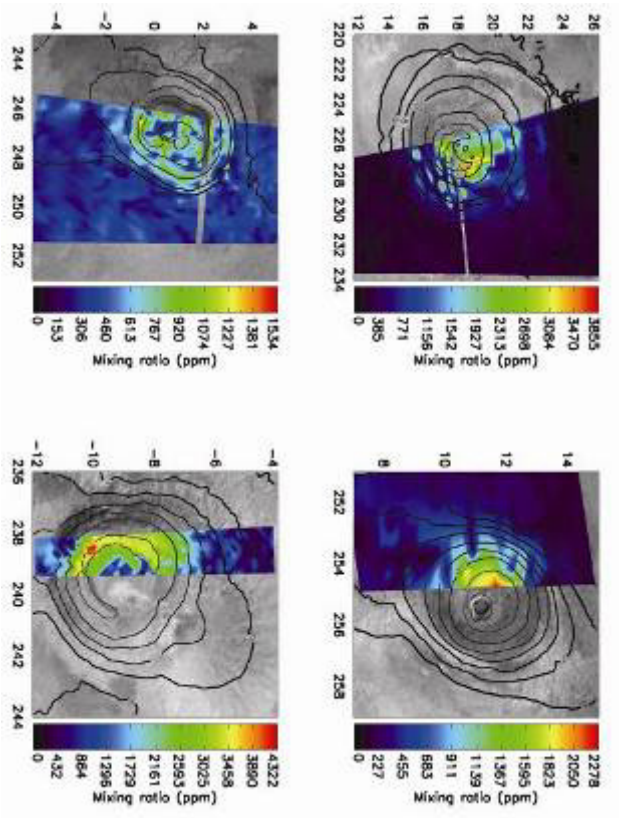

Figure 2: Atmospheric water vapour above four Tharsis volcanoes retrieved from the OMEGA observations

The behaviour of atmospheric water in the vicinity of the Tharsis volcanoes was studied with the OMEGA infrared mapping spectrometer data (Fig. 2). OMEGA observations over the volcanoes cover quite uniformly the whole Martian year, at different times of the day, allowing a complete seasonal and diurnal survey. The mixing ratio of water vapour shows a peculiar strong enrichment of up to 2000-3000 ppm on the top of the volcanoes compared to the surrounding valley, which persists for most of the year and which shows a clear seasonal trend. Such behaviour can imply confinement of atmospheric water in the lower atmosphere that indicates significant role of regolith. The reasons of such an enrichment of water vapour in the rarefied atmosphere of the volcanoes' summit is most likely

due to local circulation effects. Extreme topography of the Tharsis region and change sin thermal inertia trigger upslope winds which transport water vapour from the valley to the top of the mountains where it is absorbed by regolith or is deposited as frost. Similar studies are carried out in the regions of pronounced topography features like Hellas Basin and Valles Marineris.

1.6. Solar infrared occultation by the SPICAM experiment on Mars-Express: vertical distribution of water vapor and aerosol

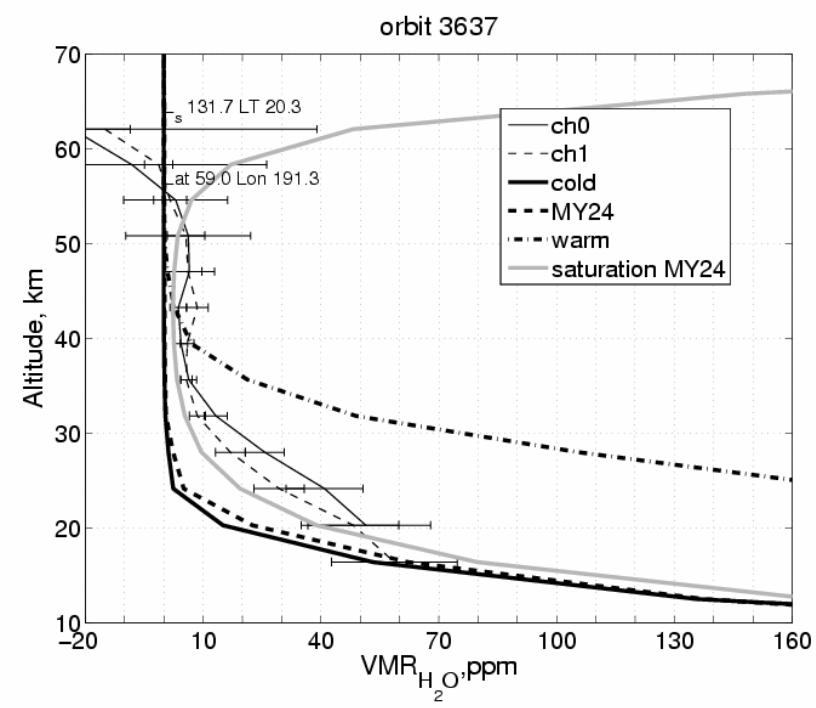

Comparison of the obtained water vapor vertical profiles (channel 1 and 2) with the prediction of general circulation model of the Martian atmosphere.

Infrared AOTF spectrometer is a part of SPICAM experiment onboard Mars-Express mission. The instrument has a capability of solar occultations and operates in the range 1–1.7 μm with mean spectral resolution of 3.5 cm^{-1}. During the two Martian years (MY 27 and 28) about 350 successful infrared occultations have been carried out, with Ls varying from 139° to 344° and full range of latitudes and longitudes. We report the first results obtained during 24 orbits in MY28 at L_S 130–160, and the latitude range of 40–55°N. For these orbits, simultaneous observations of atmospheric density from 1.43 μm CO_2 bands, water vapor mixing ratio based on 1.38 μm absorption, and aerosol opacities were retrieved. Aerosol vertical extinction profiles were obtained at 10 wavelengths in the altitude range from 10 to 60 km. The number density is found to be of the order or below 1 cm^{-3} at the altitudes between 15 and 30 km, with the effective particle radius r_{eff} ~ 0.5–1 μm. The aerosol haze top altitude does not exceed 40 km, except the orbits obtained in the range of 320–50° degrees of east longitude. In these orbits high-

altitude clouds at 50–60 km were detected with $r_{eff} = 0.1–0.3$ μm and variance $v_{eff} = 0.2–0.3$ μm, which corresponds to number density $N \sim 10$ cm^{-3}. These clouds are very poorly detectable in nadir or ground-based observations, as their vertical optical depths do not exceed 0.01 at 1.1 μm. The gas density of the atmosphere were retrieved from CO_2 band in the altitude range of 10–90 km, and H_2O mixing ratio was determined at the altitudes from 15 to 50 km. Unless very high supersaturation of water vapor occurs in the Martian atmosphere, the H_2O mixing ratio indicates by about 10 K warmer atmosphere at these altitudes than predicted by most of GCM simulations. It is faint water ice haze that may provide extra heating by absorbing solar UV radiation to maintain higher temperatures.

1.7. Ozone layer on Mars from SPICAM data

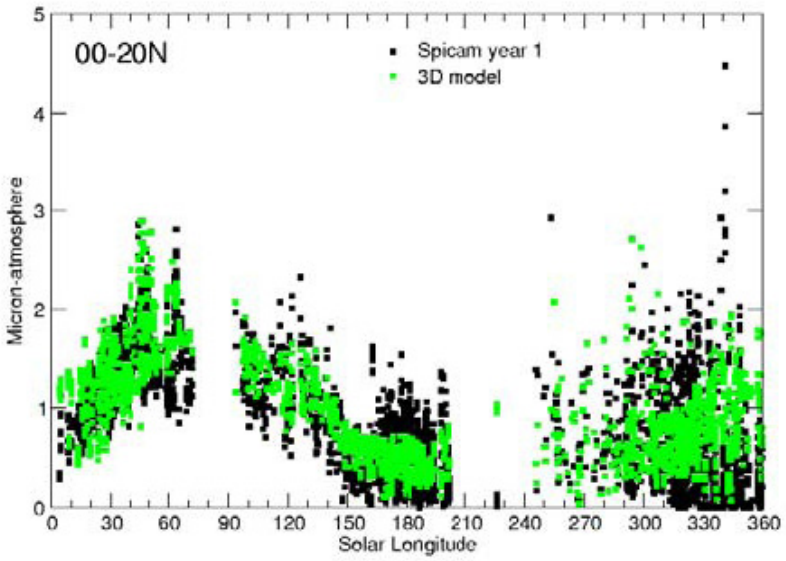

The data of SPICAM spectrometer allowed to continue the study of the distribution and seasonal variation of ozone on Mars. Seasonal and latitudinal variations and vertical distributions have been obtained and the comparison with photochemical model has been done. It is shown that the photochemical models which do not take into account heterogeneous chemical reactions on ice clouds badly approximate observations of SPICAM.

1.8. Seasonal dynamics of the water ice on the surface of the northern polar cap of Mars based on the OMEGA/MarsExpress data.

The OMEGA data contain a great volume of information including information about the polar cap dynamics. It is convenient to observe such dynamics using wide water ice spectral features (near 1.2, 1.5 and 2 μm). Since the OMEGA working range includes a series of the notable absorption bands of CO_2 and other minor atmospheric components it is necessary first of all to eliminate the

atmospheric contribution from observed spectra. That is why we have calculated spectral transmittances taking into account the observation geometry for each point of view. We used GSM (European Mars Climate Database – Forget et al.,1999) and MOLA topography. We took into account the non-uniform water vapor distribution in the atmosphere column. While zonal-averaged water vapor content from Smith et al. (2004) has been adopted, zonally variable scale height of water vapor was simulated using GFDL's MGCM(Rodin et al., 2006). Calculated atmospheric contribution was convolved with the point spread function of the instrument.

Water ice spectrum is very sensitive to the grain sizes of ice(Langevin et al., 2005; Green et al., 2007). We calculated some theoretical spectra (Fig. 1) for different effective radii of particles using model for calculation of flat surface consist of spherical particles (Mishchenko et al., 1999). The band near 1.2 μm is more sensitive to the particle size and can be the good indicator of the effective water ice particle size at the surface. At the Fig. 2 there are results of the mapping using 1.2 and 1.5 μm bands of the northern polar cap for three summer seasons of the first year of observations (we used a relative square inside the wide spectral band as the spectral index). The 1.2 μm band becomes more deeper during summer. Such effect we can interpret as seasonal changes in the microstructure of the surface of the northern polar cap: the sublimation of smaller grains takes place. Also we can see the evident zonal wave-3 and wave-4 features in the frost deposition and its evolution during the aphelion season.

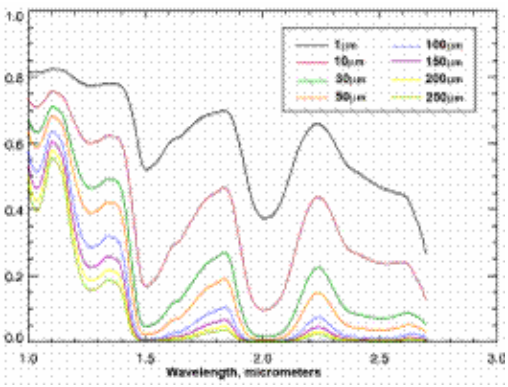

Figure 1: These theoretical spectra was calculated using model for scattering surface (Mishchenko et al., 1999)

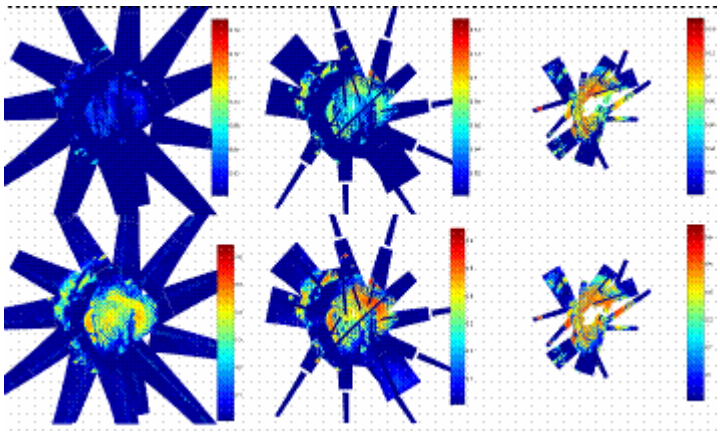

Figure 2: Maps of the water ice spectral index for 1.5 (bottom) and 1.25 (top) μm band during different intervals of the Northern summer:

1st column — L_S ~ 93-97(886-922 orbits),
2nd column — L_S ~ 113–115(1048-1060 orbits),
3rd column — Ls~127-138(1150-1216 orbits)

1.9. Season variation of temperature fields

Longwavelength channel of PFS covers a spectral range 300–1500 cm^{-1} (7–35 um) with spectral resolution 1.8 cm^{-1}. It allows to retrieve the vertical temperature

profiles from the surface up to 50–55 km. Vertical temperature profiles and aerosol opacity were retrieved from a single spectrum (at night side the temperature is low so the spectra have to be averaged). Mars Express works at near polar orbit. Each orbit data with nadir orientation of PFS enables to obtain a temperature field in coordinates latitude-altitude parallel with the aerosol (dust, water ice clouds) opacity estimation practically along the meridian at the same local time. A significant variation of spectral position of the strongest water ice band depends on the particle size, which allows to estimate it, and consequently, to determine water ice mass loading in the clouds . A seasonal variation of temperature field one may see along the orbits passing through Tharsis (Fig. Z1). Practically everywhere the ice clouds are observed, their opacity (red lines) increases from spring to summer and from morning to afternoon. The opacity τ is about 0.5 for $L_S = 27°$ and LT = 10h; $\tau \approx 2$ at $L_S = 130°$ and LT = 13h and reaches several units at $L_S = 97°$, LT = 16h. Asymmetric distribution of the water ice clouds was observed above Tharsis volcanoes. The water ice mass loading reaches maximum of 20 ppm near summit of Ascraeuss Mons (Ls=340°) on the southern flank and minimum on the Northern flank. Similar behavior is observed near aphelion for Pavonis Mons: its highest value about 60 ppm was observed at the southern flank of volcano, and the lowest one (about 5 ppm) on the Northern flank, just after summit.

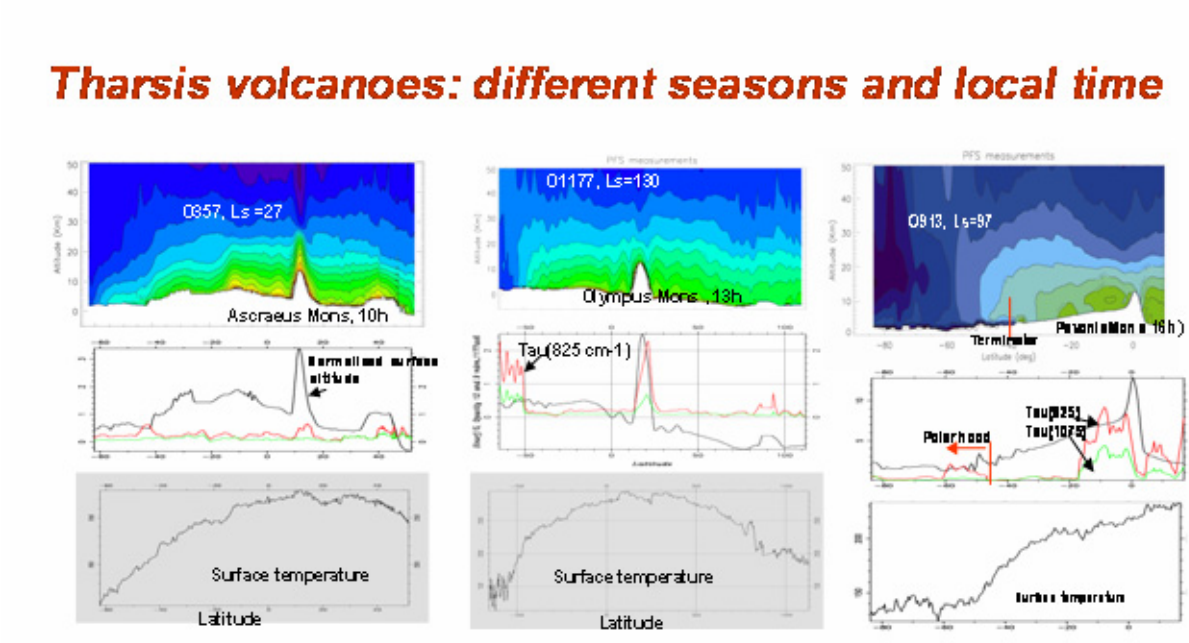

Fig. Temperature fields along the orbits through the volcanoes. Red line: opacity of the water ice clouds at 825 cm-1. Black line: normalized surface altitude. The opacity increases with the season and with local time. CO2 ice may condense on the surface in aphelion just after terminator at ϕ>40S.

1.10. Water ice clouds above North pole in aphelion

At northern summer (Fig. Z2) , during the intensive melting of the polar cap the dense ice clouds are observed above pole at $\varphi > 84°$ for the first time. These clouds are in the near surface layer. Comparison with results of GCM (Fig. Z2) show reasonal agreement in in position of the clouds (both polar and equatorial cloud belt) and water ice mass loading.

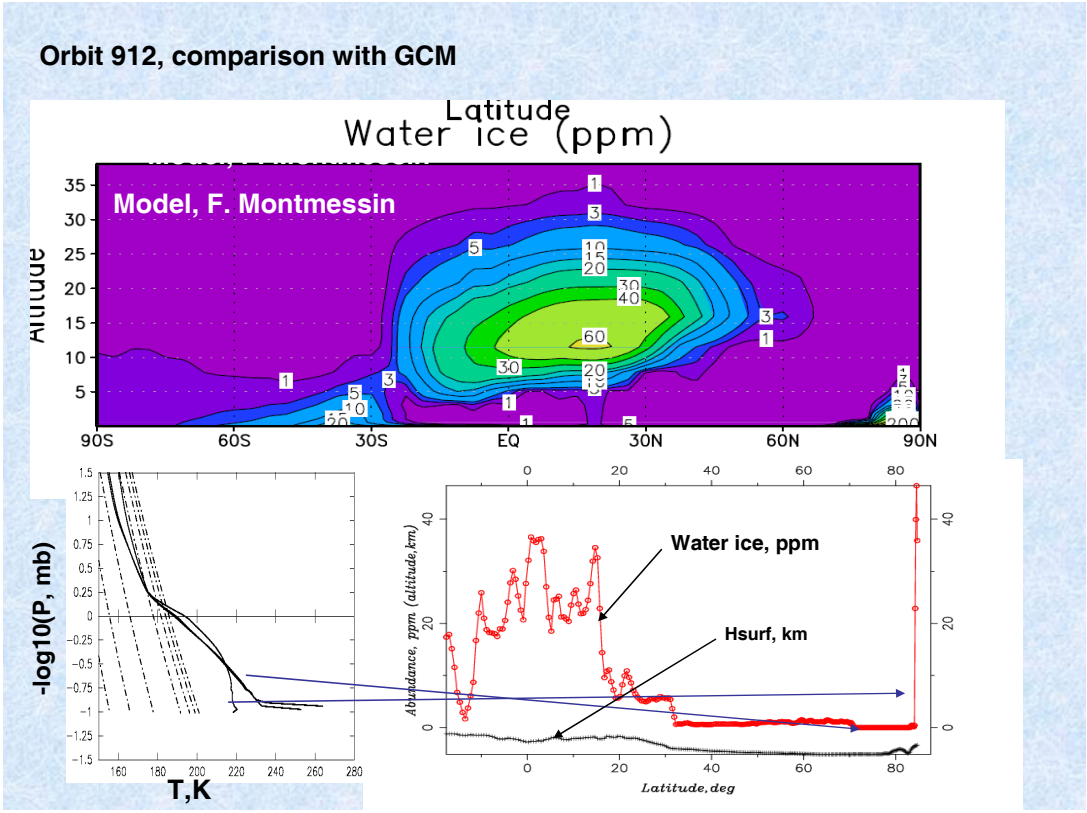

Figure: Above: H_2O abundance in water ice clouds according to model of general circulation GCM (Montmessin). Below, left: the examples of temperature profiles obtained from IR photometry for two latitudes (see the arrows). Dash-dot lines correspond to the saturation temperatures for H_2O for water abundance 0.1, 1, 10, 100, 200, 300, 400 ppm. Right: estimation of H_2O mass loading in clouds from the PFS data for different latitudes obtained near aphelion. There is a satisfactory agreement between these data and the model ones.

1.11. Structure of the atmosphere in the Northern polar region

Temperature profiles, obtained from the PFS data show that the condensation of CO_2 in the atmosphere may occur at latitudes exceeding 70°N below 20 km, where the temperature inversion is observed. The boundary of the CO_2 cap, where the CO_2 ice is observed as a condensate on the surface, is around 62N. An OMEGA image of the polar region in the O_2 1.27μm emission band reveals wave-like structures in the latitude range from around 70° up to terminator (80°). The crests of these waves are parallel to terminator, and their wavelength changes from several tens of km up to 100–150 km near terminator. Similar wave-like pattern is found in the map of the 1.43 μm CO_2 ice absorption feature and the 1.52 μm H_2O ice. Positions of these ices are anticorrelated due to thermal instability of condensation processes. Such structures may be related to gravity waves, similar to those modeled by Tobie et.al. (Icarus,164, p.33) for the winter polar night condition. Apparent column density of O_3 is obtained from the O_2 emission band at 1.27 μm. Its maximal value is found at 62–65°N. In the polar hood at latitudes $\varphi < 60°$ the O_3 abundance decreases Southward and at $\varphi = 50°$ it becomes too low to be detected by OMEGA.

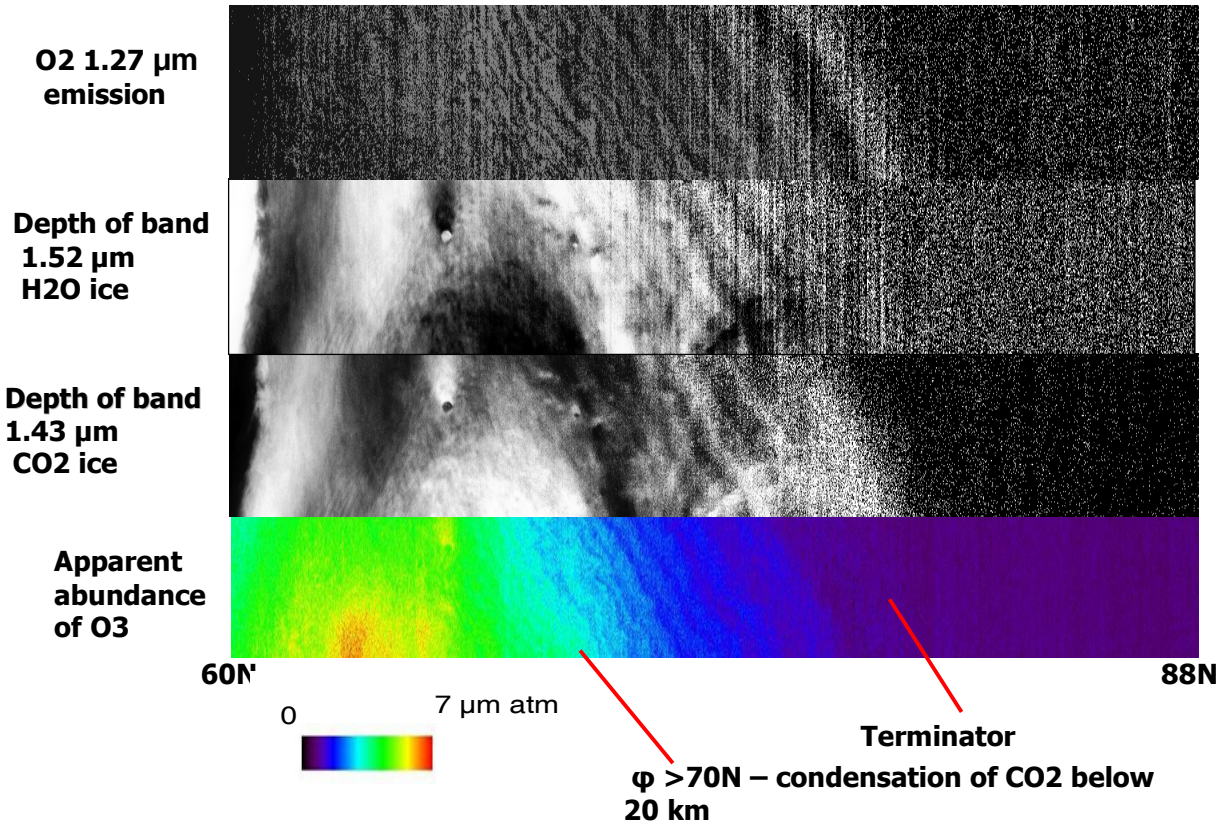

Figure: From top to bottom: Omega images in the emission band of O_2, band of ice H_2O and band of ice CO_2; the restored apparent abundance of O_3. Latitude values are shown in the bottom. Anticorrelation between the H_2O and CO_2 ices is clearly visible.

1.12. High Energy Neutrons Detector (HEND) for NASA "Mars Odyssey" orbiter (2001)

HEND instrument currently continues its scientific measurements for the 7th year on Martian orbit, all systems work properly. Basing on measurements of spatial variations of neutrons flux, HEND has detected large permafrost regions in southern and northern hemispheres of Mars with water ice composition of up to 50 %. The border between these regions lays between 40 to 60° north and south latitudes (Fig. 2). Also, considerable seasonal variations of neutrons flux were detected after measurements data was processed. This analysis allowed measuring experimentally the seasonal profile of carbon dioxide layer that falls out each autumn and winter to the planet's surface. HEND experiment data significantly specified the knowledge of modern Mars' natural environment, the model of Martian atmosphere and verified the hypothesis of global climate changes on Mars at modern epoch. HEND experiment's future measurements during the period between 2009 and 2012 will allow receiving data of Mars' neutrons flux for full 11-years cycle of solar activity, which is a very important condition to secure future manned missions to Mars.

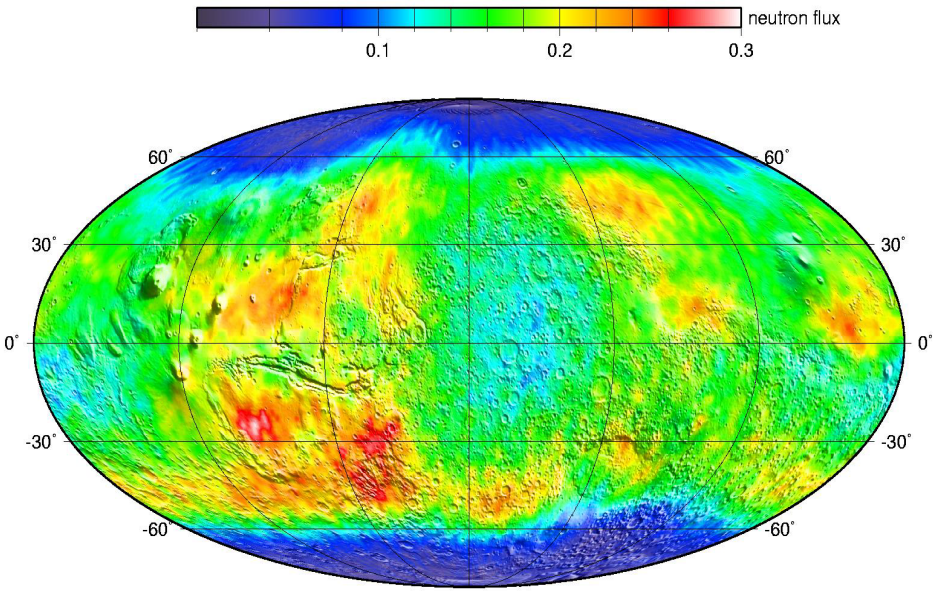

Figure 2: Map of Mars neutron flux based on data from Russian HEND instrument aboard NASA "Mars Odyssey" mission.

2. VENUS

2.1. Results of Venus exploration onboard Venus Express orbiter by instruments with Russian participation

In 2007 Venus Express orbiter continued extensive studies of Venus. In October 2007 the nominal mission that covered two Venus sidereal days was completed. The mission entered its extended phase. This work included coordination and planning of observations, as well as analysis of data from the Venus Monitoring Camera (VMC) and imaging spectrometer VIRTIS. The main results of these experiments are:

1. Observations of the global morphology of the cloud layer in broad spectral range from UV to thermal IR.
2. Observations of small scale features (convective cells, waves) at the cloud top.
3. Mapping of the cloud top altitude.
4. Determination of the wind speeds at the cloud top from tracking the UV markings.
5. Calculation of the thermal wind field in the mesosphere.

The programme of Venus Express science observations includes global monitoring from apocentre and at ascending arc of the orbit, nadir, limb and stellar, solar, and earth radio occultations. The complex programme that requires coordination between seven experiments was implemented in the Science Activity Plan (SAP) document. Particular attention was paid to the VMC observations for which a strategy of observations was developed.

2.2. Investigation of the Venus' mesosphere by SPICAV/SOIR experiment. Determination of minor constituents

Venus is veiled by a thick cloud cover of H_2SO_4 aerosol particles extending from 40 to 60 km of altitude. SPICAV/SOIR experiment performs the vertical sounding of the Venus mesosphere by means of solar and stellar occultation technique. The region 60–100 km (the mesosphere) is a transition region between two regimes of general circulation: the 4-days zonal retrograde superrotation seen at cloud top, and the solar-antisolar circulation in the thermosphere (z>100 km), with upwelling over the sub-solar point and transport to the night side. In the region 60–140 km, transport, chemistry, temperature, condensation /evaporation /aerosols all play a role in the concentration of H-bearing molecules at the altitude (≈ 80–120 km) at which they are broken by solar UV, and H atoms made available to the upper atmosphere for ultimate escape. We report the finding of an extensive layer of warm air (90-120 km) on the night side which had escaped detection up to now, and that we interpret as the result of adiabatic heating during air subsidence, which must be compensated by upwelling on the day side, transporting minor hydrogenated species upward. We also measured the concentrations of HCl, H_2O, HDO in the mesosphere. HCl is less abundant (factor ≈4) than reported 40 years ago. The ratio HDO/H_2O is enriched (factor ≈2.5) w.r.t. low atmosphere ratio and there is an unexplained depletion of H_2O around 80–90 km. These findings should give crucial constraints for dynamical and chemistry models and for estimates of the present water escape from Venus.

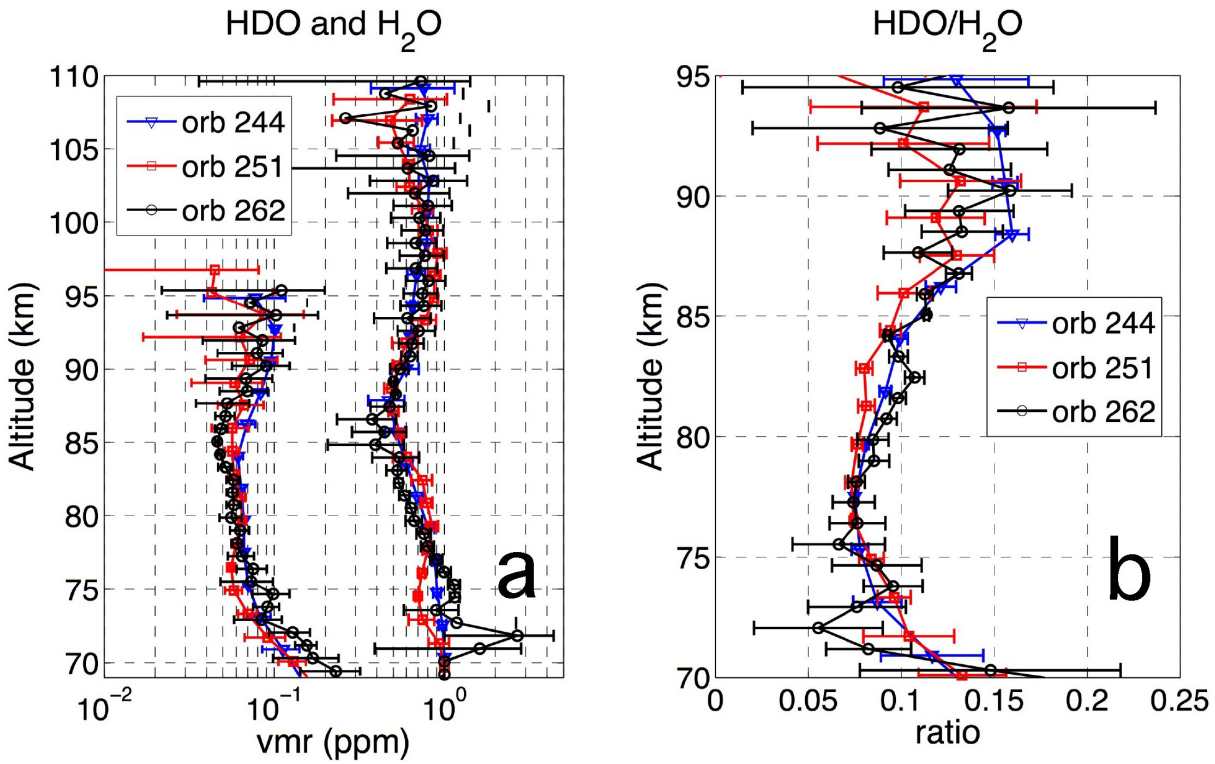

Figure: Vertical profiles of HDO, H_2O and isotopic ratio

2.3. Line parameters for the 01111–00001 band of $^{12}C^{16}O^{18}O$ (3.3 μm) from SOIR measurements of the Venus atmosphere

Absorption lines due to its $^{12}C^{16}O^{18}O$ isotopologue have been observed for the first time in Venus spectra in the 2930–3015 cm^{-1} spectral region using high-resolution spectra of SOIR. It corresponds to 01111-00001 transition. Line intensities have been determined using temperature-pressure profiles of Venus mesosphere. Line strengths of the Q-branch are in two orders higher than theoretical calculations presented in HITEMP (high-temperature spectroscopic database).

Oxygen night airglow in Venus atmosphere in the NIR spectral range

The 1.27μm O_2 $a^1\Delta g$ (0-0) airglow on the night side of Venus is produced after recombination of O atoms, which appear as the result of the CO_2 photolysis on the day side. A major fraction of these oxygen atoms is then transported to the night side via the Sub-Solar to Anti-Solar (SS-AS) circulation in the 90-130 km range of the upper mesosphere and lower thermosphere. Appearing on the nightside, the O atoms can recombine in the three body recombination reaction $O + O + M \rightarrow O_2^* + M$, with O_2^* being the excited state of molecular oxygen. The net yield for production of the $O_2(a)$ state after multiple collisions of the upper excited states has been estimated to be of 0.8 (*Gerard* et al., 2008).

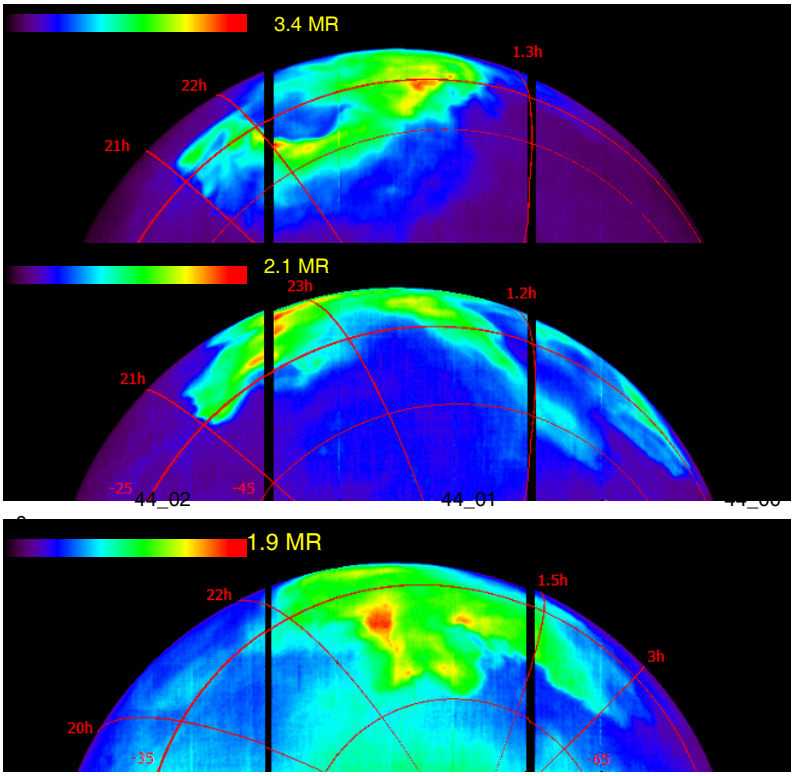

Figure 1: Intensity of the O_2 emission for three orbits. Local time and latitudes are shown. Thermal emission is excluded, angle dependence and reflection from the clouds are also taken into account. The highest intensity of the airglow is observed near midnight at low latitudes.

The emission is known to show very fast variations of its intensity and local distribution over time scales of several hours. Observations of the O_2 airglow movement in the atmosphere allow to study circulation around 100 km altitude.

Nadir observations from orbit allowed to obtain high spatial resolution of the night O_2 airglow for Venus Southern hemisphere from the equator to the polar latitudes. On the night side a window between CO_2 bands occur at 1.27 μm and the observed emission there is a superposition of the thermal emission of the lower atmosphere, scattered by the clouds, and the O_2 emission.

Vertical profile of the O_2 emission in limb view

The vertical profiles of the oxygen emission were obtained by the the retrieval of limb observation data.

The limb observations were averaged within 5° of latitude and all pixels were processed along the local normal direction. In every selected column they are then smoothed over 1 km of altitude. A typical result is shown in Fig. 2. Note that vertical profiles of the 1.27μm O_2 (0-0) emission were obtained for the first time.

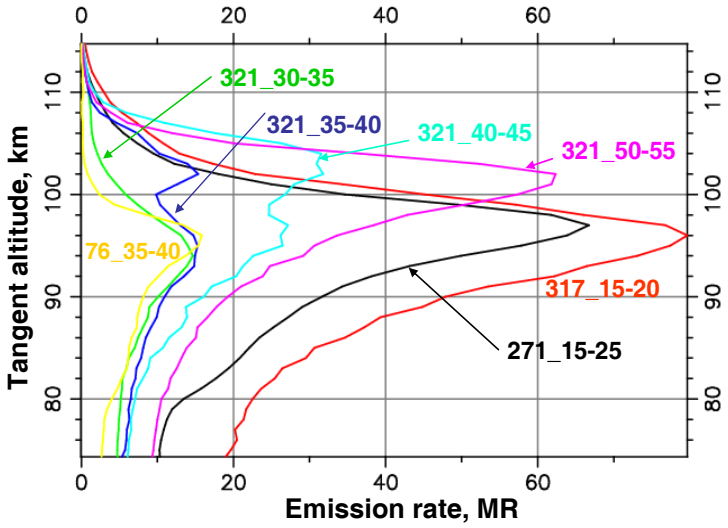

Figure: Variations of the limb profiles for different orbits. A peak of emission rate changes by an order of magnitude. The altitude of peak changes from 96 to 103 km. Numbers given near the curves mark the orbit number and the latitude range.

2.4. The 1.58 μm O_2 $a^1\Delta g$ (0-1) night glow

The 1.58 μm O_2 emission has also been measured in the VIRTIS spectra. Its vertical profile coincides with the vertical profile at 1.27 μm. The 1.27 μm/1.58 μm oxygen bands ratio have been measured and it results in a mean value of 77.9±8.7 (63±6 for the ratio of the transition probabilities A_{00}/A_{01}).

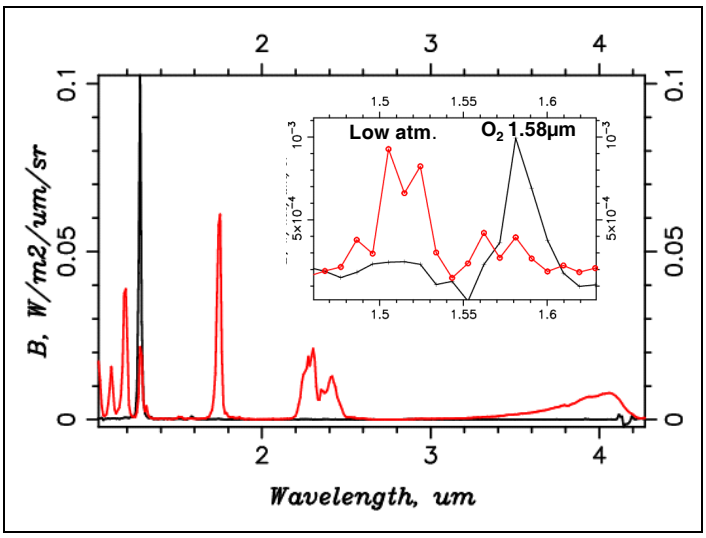

Figure: The examples of two spectra obtained by VIRTIS. Black line: limb spectrum (non-thermal oxygen emissions only are seen), red line: thermal radiation from the disc of planet, scattered by the clouds in addition to thermal emission of clouds at about 4 mkm.

2.5. Circulation in the polar dipole

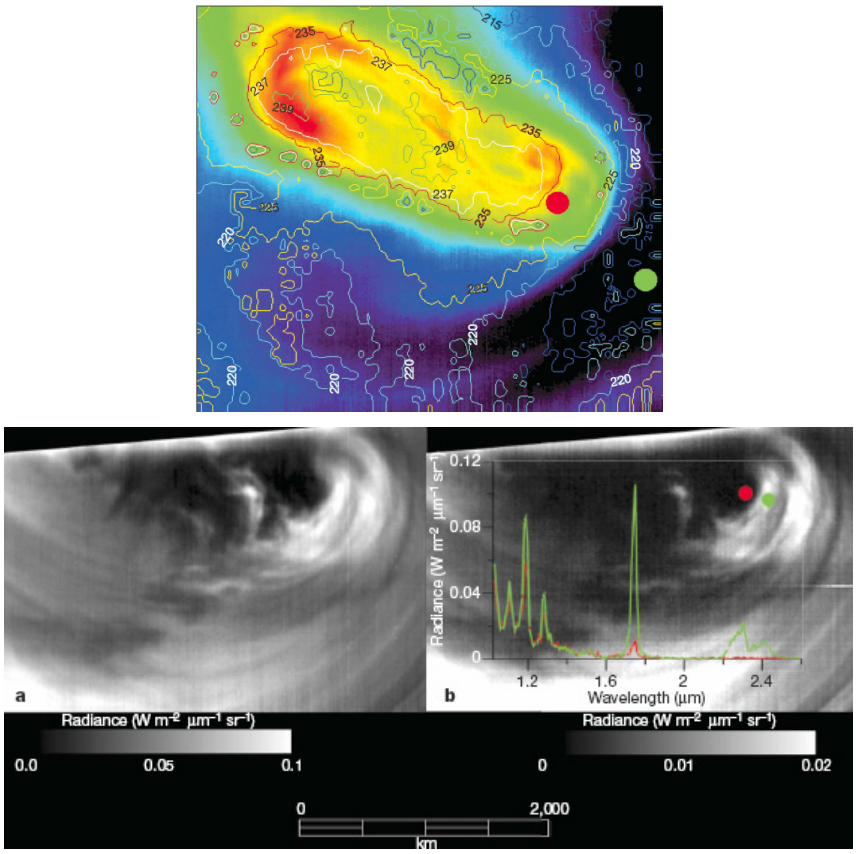

Figure: A thermal map of the south polar dipole at the altitude of about 60 km (left) and the images of the deepest layers of the clouds which scatter the radiation emitted by the lower atmosphere at 1.74 mkm (20–30 km height) and 2.35 mkm (about 50 km height).

For the first time the image of the south polar vortex was obtained and its structure was investigated in detail on the basis of VIRTIS spectrometer data . This vortex is called polar "dipole" because it has two centers of rotation. Curiously both south and north polar regions reveal similar character. Note that the north polar "dipole" was investigated earlier by Pioneer Venus and Venera 15.

The period of rotation of the south polar "dipole" was found to be 2.48±0.5 days. Both south and north dipoles are surrounded by cold polar hoods. The temperature difference between "dipole" and cold "hood "at the upper cloud boundary level may reach 50 K. Such thermal structure is caused by the dynamical properties of the atmosphere (*Piccioni* et al. 2007).

2.6. Morphology and altimetry of the cloud layer

Venus Express acquires images of Venus in broad spectral range. Figure 1 shows the image of Venus composed of VMC UV day side image and VIRTIS night side image in near-IR. Morphology of the cloud top (~70km) changes from chaotic dominated by convective cells in low latitudes to streaky structure indicating quasi-laminar flow in middle latitudes. Morphology of the polar regions shows the presence of planetary vortex several thousand s kilometer in size. Appearance of the Venus disc in UV shows strong variability at time scale of about one day that suggests vigorous dynamical and microphysical processes at the cloud top.

Observations in the near-IR range on the night side reveal the structure and dynamics deep in the cloud layer (~50 km). They also show global circumpolar vortex indicating that this structure exists throughout entire depth of the cloud. The vortex "eye" displaced by several degrees from the south pole and rotates with 2.5 days period. Both at the cloud tops and in the deep cloud periodical structures indicating wave activity were observed.

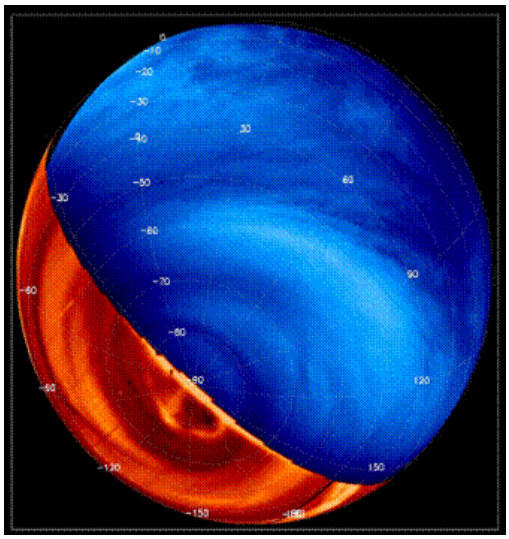

Figure: False colour image of Venus composed of the UV (365 nm) dayside image by VMC (blue) and VIRTIS night side image (1.7 μm).

Simultaneous VMC UV and VIRTIS observations in the near-IR absorption bands of CO_2 provided altimetry of the cloud top. Its altitude changes from ~70 km in low and middle latitudes to ~64 km in the polar regions.

2.7. Dynamics of the Venus atmosphere

Sequences of VMC images allow one to determine wind velocity at the cloud top from tracking UV markings. Figure 2 shows preliminary results of the zonal wind measurements. Zonal wind speed is 90±10 m/s in low latitudes quickly decreasing at higher latitudes. The measured meridional velocity was 10–20 m/s. Observations indicate diurnal variability of the wind velocity. The winds derived from UV features tracking and those calculated from the VIRTIS temperature field in cyclostrophic assumption are in general agreement. Disagreement observed in low latitudes can indicate breaking of the balance.

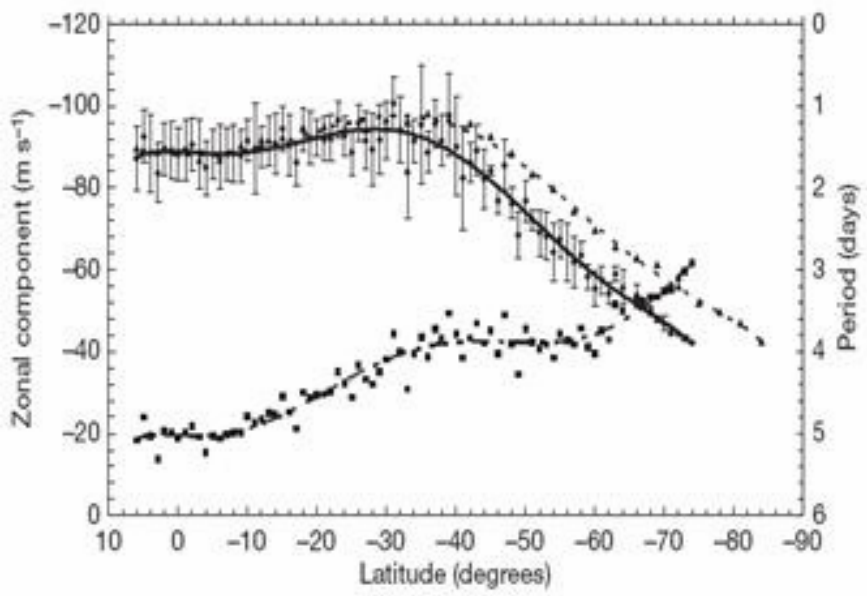

Figure: Mean zonal wind speed at the cloud top (~70 km) (solid line) and corresponding period (dashed line).

3. MERCURY

3.1. Observations of the planet Mercury and their interpretation

Astronomical observation. During the May 2007 and November 2007 elongations, in the SAO observatory the Russian Academy of Science (position of the observatory is 41°26'E, 43°39'N) new observations of Mercury were carried out in position of the planet, allowing to document the areas which have been not covered with MARINER-10 imaging in 1974-75. The CCD camera STV has been mounted on the Zeiss-1000 telescope (Figs. 1, 2). In the autumn elongation it was supposed to use more perfect SAO CCD camera instead the old one. As against

observation of the previous years, the continuous sequence of the video frames with the real time AD-conversion and recording on a hard disk of a computer was used. This method considerably increases efficiency of observation. Unfortunately, in both elongations (May and November) a successful observation was not possible because of the extremely adverse meteorological conditions.

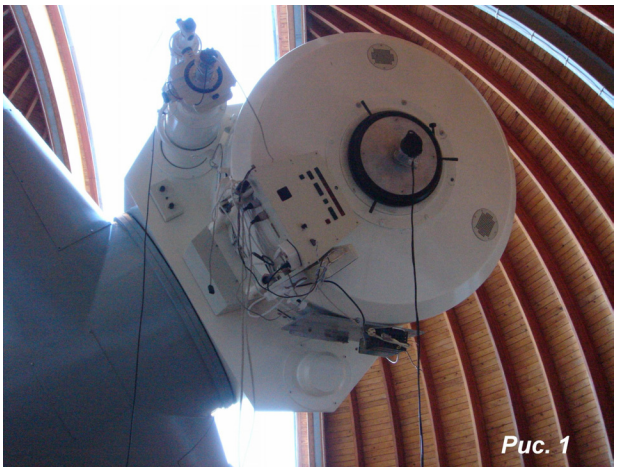
Рис. 1


Рис. 2

It is possible to attribute to experimental works a development of new programs of processing the saved observant material got up earlier: codes ASTROSTACK 3 and programs RegiStax 2. Transition from 8-digit bmp-format to 16-digit raw is supposed, will raise the resolution and clearness of fine details of images. This work is not completed yet.

Impact craters in 210–285˚W sector. The paper of L. Ksanfomality, A. Sprague. <New images of Mercury's surface from 210° to 290° W longitudes with implications for Mercury's global asymmetry> (ICARUS, 2007. 188. p. 271–287) presents new results of processing of images of Mercury acquired during the 2002 spring evening elongations. A new step in of the resolution progress (Fig. 3) has allowed proceeding to map districts of largest impact craters on the surface of Mercury. Some of them are similar to ring structures, but have no rays. At the same time, craters with extended rays are seen in many areas of a planet (e.g., at 8ºS, 265ºW). The big crater with a ray system is placed at 10ºS, 247ºW, where its west borders surround the second brightest area of this hemisphere of the plane, in the given phase (see Ksanfomality, Astronomy letters, 2005, V. 31, №11, p. 860–880, <The Resolved images of unknown sector of the surface of Mercury>). Light areas form here an arch or, may be, a ring formation having a diameter of 600–700 km. Using a selective increase in contrast, makes numerous impact craters appreciable. A

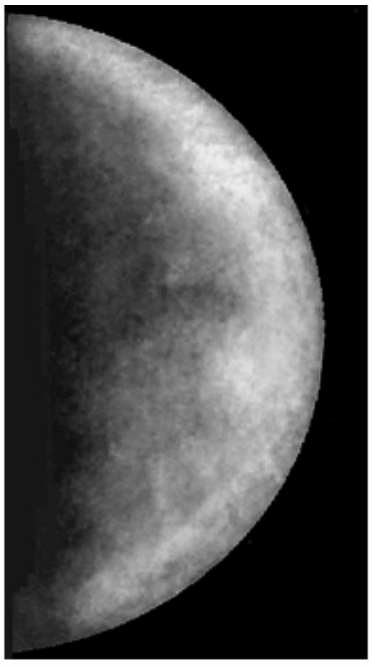
Рис. 3. 210-285°W.

crater with a diameter 140 km and a rim of debris having 450-500 kms in diameter around it, with the center at 21ºS, 248ºW, is those. Probably, sites adjoining to a rim outside, are debris from the crater. Similar craters are met practically in all areas of the 210–290ºW sector. On Fig. 4 there are 5 large impact craters (chosen from the initial Fig. 3), undoubtedly, of a shock origin, by the sizes from 400 up to 800 km. During the observation they were located on the terminator and consequently are most contrasted. Arrows connect an initial position of areas with their enlarged (2:1) contrasted images. The side of squares on Fig. 4, where craters are shown, makes 900 km.

All craters have wide terraces of debris. Statistically sizes of Mercury impact craters are 1.5 times less than lunar, that speaks twice the big acceleration of free falling. In all versions of the synthesized images the northern horn, at the pole, has a large shock crater (see Ksanfomality, Astronomy letters, 2005), with an extensive rims of debris, and diameter about 6º (280 kms). Its central dark part has a diameter about 2º (90 kms). The wreath of the crater is appreciably brighter than surrounding details and is allocated on their background. 2–3 degrees closer to the North pole, on its northern side, there is a smaller crater, about 60 kms. The latitude coordinates of a large crater is 85ºN. At the moment of observation the North pole was few degrees closer to the observer, than a limb, therefore the zone of the pole was visible. Because of affinity to a pole and some blurring of the limb, the longitude of craters in a zone of pole of Mercury is determined with a probable error not better 5º. But position of craters managed to be compared to the independent data: the area of North Pole is known by a detailed radar map, showing a group of large impact craters, with a resolution up to 1.5 kms (Harmon et al., 2001). Apparently, these craters are visible on our synthesized images, too. Their comparison with the radar map shows that the sizes and position of the 85°N crater coincide practically completely with the radar crater at the radar map (the center is 85.5°N, 292°W, diameter about 80 km). It is interesting, that the wreath of debris on the radar map is seen only from northern side of the crater, without details, while in the optical image the terrace of debris surrounds the crater around, and the wreath is visible as bright formation. High brightness of debris from crater K can be compared to features of the craters shown on the radar map of the polar area. Following Harmon et al., 2001, craters at the pole are unusual by their nature. On their bottom, under a layer of regolith, there are, apparently, big masses of ice. The bottom of polar craters always remains in a shadow of the rim and has the temperature low enough that ice was kept for cosmogonic time. According to an other hypothesis, at the bottom of craters there is adjournment of sulfur (Sprague et al., 1995), which in a decimeter radar range has characteristics alb of scattering similar to ice. In our case another thing is important – it is possible that their high edo is connected somehow to the craters nature.

The available experimental data show actually that Mercury's craters morphologically differ from the lunar. For the second craters on Fig. 4, there is only one analogue on the Moon – crater Wargentin, on the Moon's Western limb. Many experts count it to be uplifted feature filled by lava.

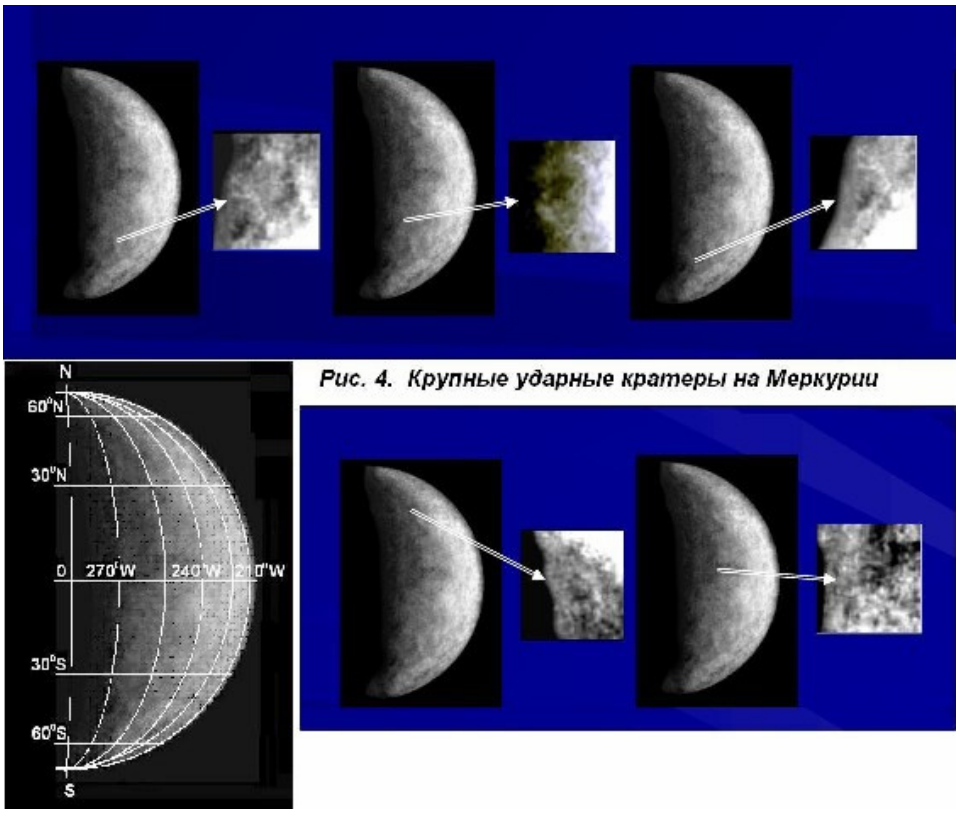

Рис. 4. Крупные ударные кратеры на Меркурии

Data processing of 2006. As it was already specified in published papers that expositions at morning elongations much more improve the resolution of astronomical images (L. Ksanfomality, Astronomy letters, 2005). Pertinently to remind, that though the short exposure idea of increase of the resolution of astronomical images existed for a long time, only the advent of CCD devices with their high quantum efficiency makes possible obtaining resolved images of Mercury, by processing a large number of electronic photos that were made by the method of short expositions. Unsurpassed result there is an image of sector of longitudes Mercury 270–330°W, Fig. 5. Still it was possible only preliminary processing of the acquired data to fulfill. The result is presented on Fig. 6. New images of a surface of a planet, Fig. 5 and 6, cover a significant part of surface Mercury, remaining not imaged by the MARINER-10 camera. They prove to be true, that extended details of a relief, apparently, are asymmetrically distributed on the surface of Mercury.

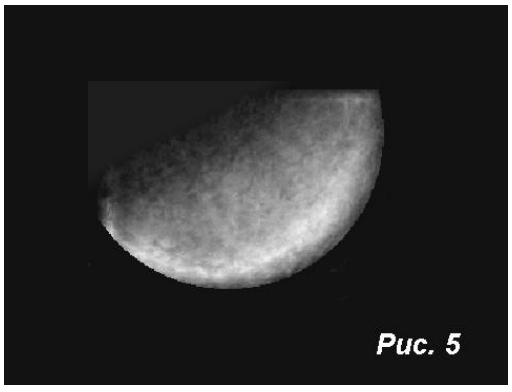

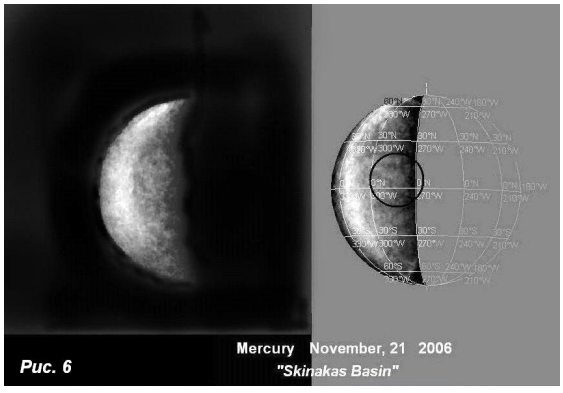

Рис. 6

3.2. THEORETICAL AND EXPERIMENTAL RESEARCHES

On the basis of a radar method suggested by I.V.Holin (1988, 1992, 1999), by means of the interferometer Goldstone — Green Bank (USA) were measured by a radar-location components of an instant spin-vector of Mercury, an inclination and amplitude 88-day librations of Mercury. Simultaneously the conformity of Mercury to the Cassini state (Margot et al., 2007) was checked. Essential deviations from the Cassini state was not found, and the obtained values for an inclination and amplitudes make 2′1 ± 0′1 and 35″8±2 ″ accordingly (instead of former 60″±6″). Based on that the conclusion made about the libration of the shell separately from the core has been made. It means the presence of liquid phase in the core (*Margot* et al., 2007). I. Holin states that publication Margot et al. (2007) it is not free from essential losses. Among them there is a deformed historical description, a number of discrepancies with known works (Green 1968, George 1976, Holin 1988, 1992, 2004) and absence of due discussion with co-authors. Achieved accuracy seems is appreciablly lower than the theoretical limit, established by Holin (1992). The results of the work could be carefully verified.

The work of Margot et al. (2007) is first practical use of the Holin method (1992), which can promote considerable progress in research of Solar system. The opportunities connected to a possible creation of a new planetary radar in Euro-Asia where due to set of already available radiotelescopes (mainly in Europe) accuracy considerably grow (Van Hoolst et al., 2007). considered. One of suggested possible places for a creation of a radar-tracking complex is Northern Caucasus.

2.2.1.2. Works on Space Research in Progress

High Energy Neutrons Detector (HEND) for NASA Mars Odyssey orbiter (2001)

Figure 1: Mars Odyssey spacecraft with HEND instrument on it's deck.

Fast neutrons detector HEND is a Russian experiment making part in the Gamma-Ray Spectrometer instruments suite aboard NASA Mars Odyssey (Fig. 1). HEND's scientific goal is to study neutron emission from Mars to search for water and to measure the elementary composition of chemical elements of Mars' soil (based on coordinated data processing with GRS instrument's gamma ray measurements). A map of neutron component of Mars' radiation is also to be built based on measurements data. The HEND instrument was ordered by Russian Federal Space Agency and created at the Space Research Institute (prof. Igor Mitrofanov is HEND PI).

Onboard Telescope for Neutrons BTN-M1 on Russian Segment ISS

After HEND experiment successfully started its operations onboard NASA's "Mars Odyssey" orbiter, a decision was taken to install spare flight instrument onboard of Russian Segment of International Space Station as part of "BTN-Neutron" experiment's first stage. BTN-M1 instrument that measures neutrons flux on orbit near Earth was developed based on the usage of HEND instrument. The neutrons, measured by the instrument are produced by upper layers of Earth's atmosphere and the body of ISS itself under the influence of cosmic rays. BTN-M1 instrument will also measure direct neutrons emission from powerful solar proton events that are accompanied with heavy nucleus acceleration in Sun's active regions.

Figure 3: Russian cosmonaut M. Turin and US astronaut M. Lopez-Alegria installed BTN-M1 instrument on board IIS.

BTN-M1 was created at the Space Research Institute under the order from Rocket and Space Corporation "Energia" (experiment PI is prof. Igor Mitrofanov). This instrument was delivered to the IIS in October 2006 by Progress M-358 vehicle. Then, in November 2006 M. Turin, cosmonaut of expedition IIS-14 accomplished the installation and connection of the BTN-ME module. BTN-MD module was prepared to be carried out into open space. It was installed on its place during two

EVAs by M. Turin and M. Lopez-Alegria, another astronaut of expedition IIS-14 on November 23d, 2006 and February 22d 2007 (Fig. 3). On February 26 2007, the instrument was powered on and set to scientific measurements mode.

During all the period of work in 2007, the instrument functioned properly with all parameters within acceptable limits. An interplanetary network for radiation environment monitoring synchronously on Martian (Mars Odyssey) and Earth (IIS) orbits is created and will allow to predict radiation conditions along the entire path of interplanetary flight from Earth to Mars and back to Earth. Based on measurements data from BTN-M1 instrument a map of radiation dose from neutrons flux acceleration rate in different ISS locations was created (pic. 4). The particularity of this map is the dose increase observed in the South-Atlantic magnetic anomaly region. During the period of measurements in 2007 and 2008 this radiation background particularity in near Earth's space was the most noticeable as this period concurred with low solar activity period.

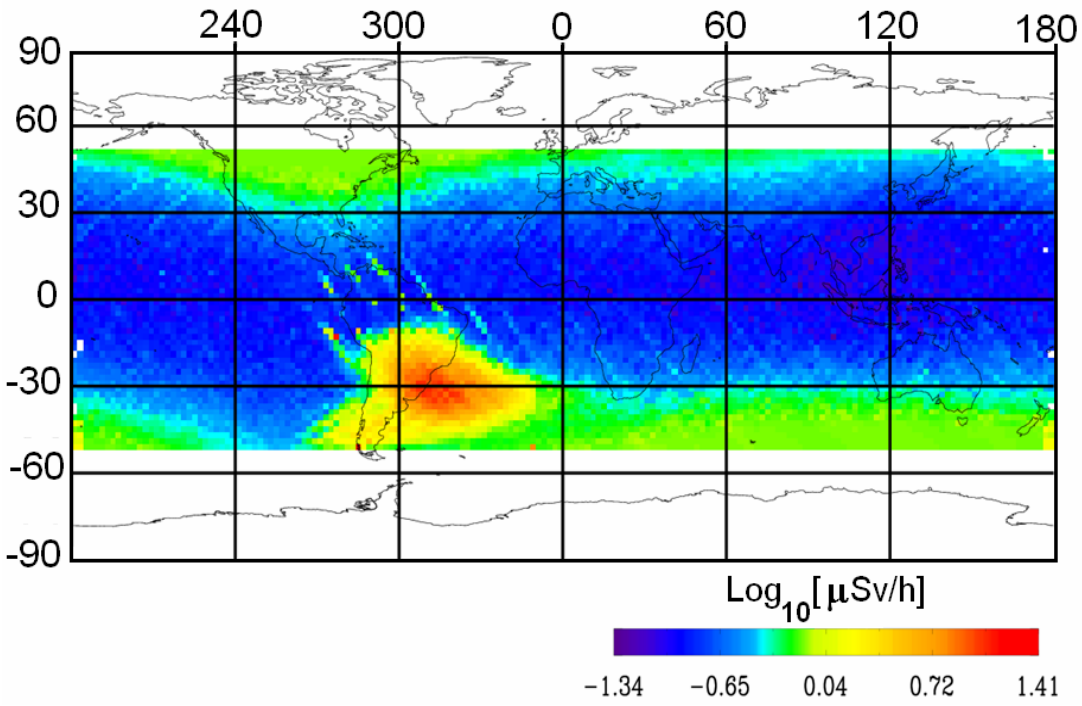

Figure 4: Map of radiation dose from neutrons flux acceleration rate in the near Earth's space based on data from BTN-M1 instrument measurements onboard IIS in 2007.

Experiments onboard the "Mars Express" ESA mission

In the frame of Federal Space programme Roscomos has funded the development of components for three scientific instruments for ESA Mars Express spacecraft. Mars Express orbiting Mars since 25 december 2003. In Russia, in IKI the front-end optics and the scanner system of mapping spectrometer OMEGA, detectors and calibration equipment of Fourier-spectrometer PFS, and the infrared channel of versatile spectrometers SPICAM have been developed and manufactured. The

Russian participation in experiment planning is also supported by Roscosmos. Presently all the three spectrometers are operating nominally; and their measurements allowed a number of new scientific results. During 2007–2008 Russian members of science teams of these experiments have published more than 10 papers in refereed literature. ESA plans to support the operations of Mars Express up to May 2009.

Experiments onboard the "Venus Express" ESA mission

In the frame of Federal Space programme Roscomos has funded the development of components for two scientific instruments for ESA Venus Express spacecraft, orbiting Venus since April 2006. In Russia, in IKI the detectors and calibration equipment of Fourier-spectrometer PFS, and the infrared channel of versatile spectrometers SPICAV have been developed and manufactured. These instruments are close analogues of Mars Express PFS and SPICAM instruments adapted for the studies of Venus. In addition to joint experiment SPICAV (France, Russia, Belgium) a completely new experiment, high-resolution echelle-spectrometer SOIR has been proposed by Russian scientists and developed in cooperation among Belgium and France. SPICAV-SOIR instrument is operating nominally; PFS is not performing Venus observation because of scanner malfunction. The science objectives of PFS are partially recovered by means of VIRTIS imaging spectrometer. The results of nominal mission of Venus Express are published in a special section of Nature journal in 29 november 2007. Russian members of science teams of Venus Express experiments have published more than 10 papers in refereed literature, including 5 in Nature. ESA plans to support the operations of Mars Express up to May 2009, with a possible extension until 2011.

Experiment Miniaturized Moessbauer Spectrometer (MIMOS) onboard the "Mars Exploration Rovers" NASA mission

The Miniaturized Moessbauer Spectrometer (MIMOS) was proposed in the beginning of 1990s by scientists from Space Research Institute for Russian Mars-96 mission. It was developed at Darmstadt Technical University and Johannes Gutenberg University of Mainz, Germany in collaboration with Space Research Institute.

Mössbauer spectroscopy is a powerful tool for investigation of iron-bearing minerals. It provides quantitative information about the distribution of iron among its oxidation states and its relative abundance in iron bearing phases. Two MIMOS instruments are part of the Athena scientific payload on board NASA's twin Mars Exploration Rovers "Spirit" and "Opportunity", landed on Mars in January 2004. Originally constructed for a three months mission, both rovers and both Moessbauer spectrometers are still operational after more than four years of exploring the Martian surface (more than 1500 local days - sols) and continue to return valuable scientific data.

"Spirit" has traversed the plains from her landing site in Gusev crater and is now, for the greater part of the mission, investigating the stratigraphically older Columbia Hills. Olivine in rocks and soils in the plains suggests that physical rather than chemical processes are currently active. Hematite and goethite identified in rocks at the West Spur of the Columbia Hills by Moessbauer spectrometer show that water played a major role in the formation and alteration of rocks and soils in the Columbia Hills.

"Opportunity" has landed at Meridiani Planum. The ferric sulfate hydroxide mineral jarosite was identified in sulfate-rich outcrop rocks by MIMOS. Millimeter-sized spherules were identified as the source of hematite detected from orbit. Mössbauer data were crucial to identify in Bounce Rock the first rock on Mars itself similar in composition to basaltic shergottites, a group of meteorites whose origin is believed to be Mars. The identification of the iron nickel alloy kamacite in Heat Shield Rock and Barberton revealed an iron meteorite and a stony meteorite, respectively, the first to be discovered on Mars.

Observations using the "INTEGRAL" International observatory

International Gamma-Ray observatory INTEGRAL was launched by Russian Proton rocket on October 2002 into a highly eccentric orbit. In exchange for this launch russian scientists have got priority rights for the use of 25 percent of observation time aboard the observatory provided by Russian Scientific Data Center (RSDC) for INTEGRAL project, organized in the Space Research Institute (Moscow). From the moment of RSDC creation its employees actively working on adaptation of existing and development of new software of the mission, they are engaged in distribution of the information on the project among the Russian scientific community.

Within five years of work at the orbit INTEGRAL observatory has collected a huge amount of observational data that has allowed to start investigations demanding long expositions. First of all there are the problems connected with processing of all available observatory data, such, as execution of deep all sky survey, search of weak sources populations of the Galactic and extragalactic nature, detailed research of radiation in nuclear lines, etc. Gradual filling of RSDC archive with observational data and sharp growth of its processing have demanded essential increase in computing capacities.

Owing to the financial support received from the Russian Fund of Basic researches, and also funds of Space Researche Institute, the new equipment for storage and processing of INTEGRAL observatory data has been purchased. In a special premise of the Space Researche Institute operational center the modern information complex consisting of the Sun Microsystems corporation <http://ru.sun.com/> equipment has been mounted. The data storage with a high degree of reliability and availability will be realized on SunFire X4500 server http://ru.sun.com/products/servers/entry/fireX4500/index.html with the size of disk space more than 20 terabyte, that, in aggregate with already available equipment,

has allowed to finish total capacity of archive almost up to 30 terabyte. Besides functions of a data storage new server possesses also high computing characteristics owing to two double-core AMD Opteron processors. Additional computing capacities of information complex is provided with SunFire X2200 server http://ru.sun.com/products/servers/entry/fireX2200/index.html on the basis of two double-core AMD Opteron processors.

2.2.2. V.A. KOTELNIKOV INSTITUTE OF RADIO ENGINEERING AND ELECTRONICS OF THE RAS

2.2.2.1. Information System of Operational Data in NTS OMZ (TERRA-MODIS Data Processing)

The main components of the information system of the Earth remote sensing satellite data, which is under development in NTs OMZ in cooperation with FIRE RAS, are described. The main accent is made on the subsystems for data storing and data access in application to the MODIS TERRA data processing.

Introduction

A large amount of information which is receiving by means of Earth remote sensing satellites requires an adequate information system for data processing, cataloguing and archiving of this information and the retrieval results. The data collected in the information system may be used as for operational as for fundamental scientific and applied investigations [1–3].

The main elements of the information system are the subsystems for storing data and for data access. These subsystems must provide a required level of reliability of data keeping and efficiency of data access. As a rule such systems are directed to requirements of the end user. So, this information system must have a simple, comfortable and easy to use interface, which provides for user all required functions, but at the same time it must not permit to do any unhallowed tasks.

Information received from Earth remote sensing satellites is stored in the centers for data processing and storing. Now in Russia there are several centers, such as http://smis.iki.rssi.ru/archive — IKI RAN; http://ire.rssi.ru/cpssi — CPSSI IRE RAS, Fryazino; http://sputnik.infospace.ru/catalog_eng.html — SRC “Planeta”; http://ckm.iszf.irk.ru/satdata — Regional center ISZF SO RAS, Irkutsk and other. Data stored in these centers usually have some thematic orientation.

An integral part of the data processing and storing centers is information system, including modern hardware and software tools for reliable and long time storing the data and corresponding graphical interfaces, which allow user to query and to obtain required information [2, 4].

One of such centers for data processing and storing the space information is the Research Center for Earth operative monitoring (NTs OMZ) of the Russian Space Agency (Roscosmos). Information system creating in NTs OMZ is oriented to provide the solution of general tasks, which are in responsibility of the Federal level Earth remote sensing center. In particular there are: management of the State archive of Earth remote sensing data and providing users with the possibility to search and receive required information [5].

In this paper the main attention is made on description of the operation of NTs OMZ information system on processing, cataloguing and archiving the data from MODIS device on the USA satellite TERRA. Polar orbiting satellite TERRA was launched December 18, 1999. MODIS device is a medium resolution scanning spectroradiometer with 36 spectral channels in 0.4-14.4 mcm band (http://modis.gsfc.nasa.gov/).

Brief Description of the Information System

Information system in NTS OMZ includes the following functional subsystems:

- satellite data acquisition and archiving in operational archive;
- data processing to level 1b[1] (radiometrically corrected and calibrated in physical units at full instrument resolution as required);
- cataloguing the information in the specially developed data base (DB);
- creation of long live archive on the DLT tapes;
- creation of the data exchange system via Internet.

Information system infrastructure consists of complex of catalogues of satellite data archives and software and hardware means for catalogue and ancillary information exchange. This infrastructure allows making search of the general and detailed information, and after that to order the required data in frame of the same system.

At present time in NTs OMZ there are archive end electronic catalogue of the data received from Russian and foreign Earth remote sensing satellites. There is a possibility for remote access to the catalogue via communication channels and Internet. Now the creation of the software and hardware complex for long time data archive and cataloguing support is under completion.

The data from TERRA satellite are receiving in NTs OMZ in the mode of direct downlink and are storing in the operational archive. The data are in the PDS format (product data set). For the data processing a software package IMAPP (International MODIS/AIRS Processing Package) is used. It is developed in Wisconsin University under NASA support and is standard for MODIS data processing. This software converts the data from raw format level 0 to the standard products of level 1a and 1b. This converting includes also calibration and geographic referencing of the data.

Software components of the NTs OMZ information system

In NTs OMZ information system the Oracle data base management system (DBMS) is used.

[1] According to the definition suggested by EOSDIS and adopted by CEOS.

The developed data base consists of two main parts. The first one is used for storing the descriptions of data collections of satellite data, and the second one for storing detailed descriptions of all minimal portions of archived data (granules).

Data processing, cataloguing and archiving of the received information is conducted in the automatic regime. Specially developed software for these purposes includes:

1. Software for data exchange between computers of the system:
   a. ftpx – data transfer from operation archive server to the data processing subsystem;
   b. ftpput – data transfer from data processing subsystem to the archive.
2. Software for registration of input satellite data entered into data processing subsystem.
3. Software for cataloguing the data entered into long time archive.
4. Software for making backup copies of data collections and recording them into magnetic tapes (DLT).

Software components 2–4 and IMAPP package are managed by special supervision program MODIS_OMZ.pl.

Software tools providing data search and data order functions are installed in web server NTs OMZ (http://sun.ntsomz.ru/data_new) and are the integral part of the whole information system http://www.ntsomz.ru.

Data request subsystem of the NTs OMZ information system

One of the main user requirements to the information system is decreasing of the time costs on data search and data obtain. In application to the satellite data the important condition of the search system is a requirement to provide querying all the data sets included into information system simultaneously. To provide such possibility a data request subsystem has special user interfaces (access gateways) to the descriptions of archived data. These gateways allow organizing process of search, view graphical primitives and order required data in the same graphical interface. The important feature of data request subsystem as general is provision users with actual information about archived data. This is possible because user interface has direct connection to the data catalogue, content of which is synchronized with archive descriptions. Moreover data search system not allowed to make user contradictory request even at the beginning stages.

For a detailed search, it is required to define the following attributes:

- **Geographic region** — geographical coordinates of the interest region defined by rectangle with longitude (± 180 deg.) and latitude (± 90 deg.);
- **Date-Time** — data and time of the beginning and the end of interested measurements;

- **Project** — project name (name of the program or mission) in frame of which measurements were conducted (values are selected from a valid list according to archive content);
- **Instrument** — instrument name, data from which are stored in the granules (values are selected from a valid list according to archive content).

As a search result, user at first receives list of data sets and, after that, a list of granules matched to selected search criteria.

Each granule, obtained as a search result, has so called browse images (NASA) or quick look (ESA). Browse images are mostly intended for visual control of data quality as for measurement quality (such as sun angle, cloudiness conditions, etc.) as for data distortions in process of data downlink, and other. User interface allow viewing these browse images and select requested granules according to the results of visual analyses.

In conjunction with a search and visual control of data quality, interface of data request subsystem allows user to make an order on selected granules immediately after data search and selection process in the same working session.

Order creation includes two actions:

1) Selection of data transfer option;
2) Registration of contact information about user.

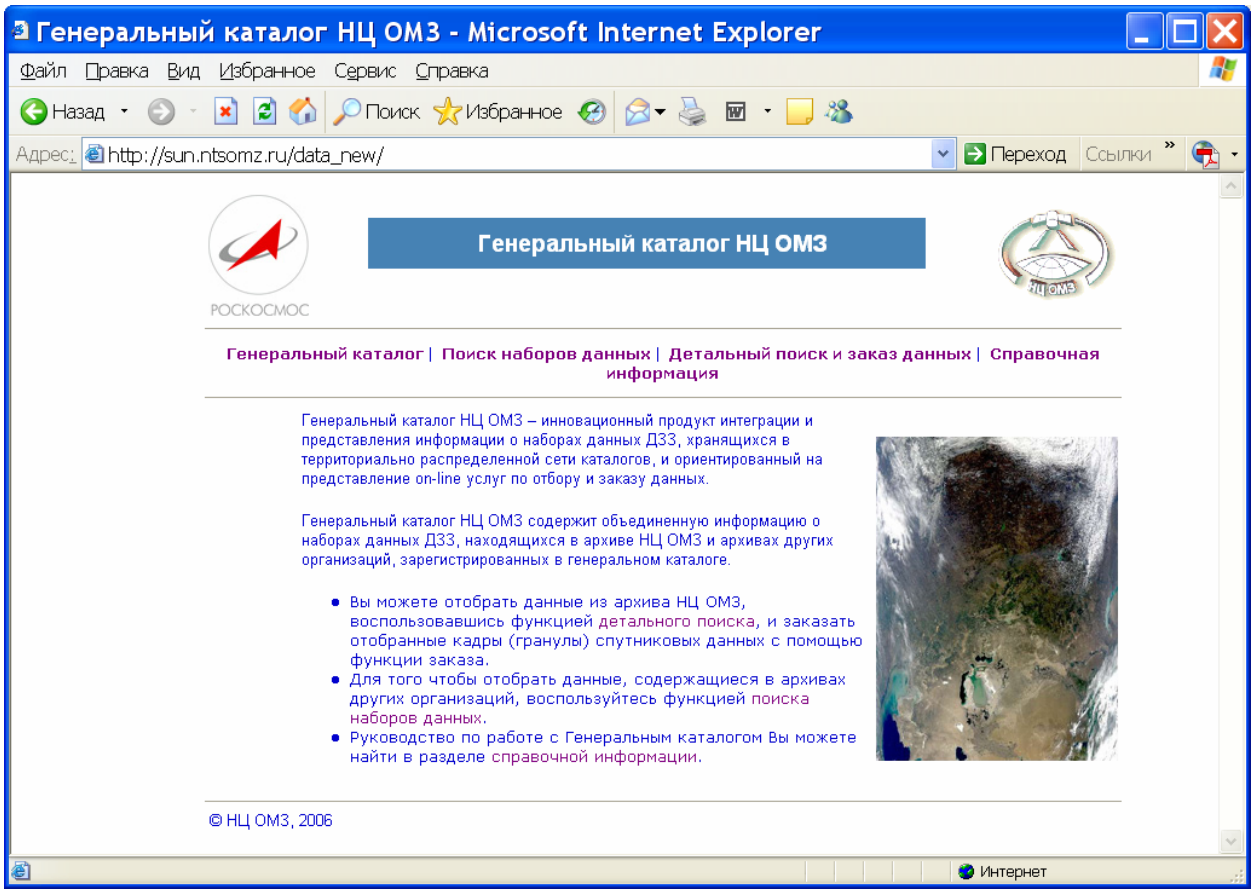

Selection of data transfer option includes a choice of the media type for recording a requested data and preferable data format. Created order is automatically transferring to the data archive. Simultaneously a request for order confirmation is send to user via e-mail. As a rule, order begins to execute in archive only after receiving an order confirmation from user.

Data request subsystem is developed with use of free of charge software packages and libraries available for Solaris operation system. The basic part of it is Web server Apache with PHP module. PHP module has enough flexibility to dynamically generate a request forms, presentation of search results forms and has internal tools for Oracle database access. Moreover it allows using graphical library for dynamic generation of the images, for drawing a vector elements (polygons, cycles, etc.) and text comments on images. Used software packages and libraries exist for other computer operation systems such as Windows and Linux. So, such configuration allows transferring the developed software to another computer platform with minimal cost, mostly associated with a configuration tasks.

The main page of data request subsystem is presented in Fig.

2.2.3. V.I. VERNADSKIY INSTITUTE OF GEOCHEMISTRY AND ANALYTICAL CHEMISTRY OF THE RAS

Mars Global Surveyor and Mars Odyssey: US missions to Mars

2.1. *Analysis of data of the neutron survey by Russian instrument HEND on board of Mars Odyssey spacecraft and data of thermal mapping of Mars by TES instrument onboard of Mars Global Surveyor spacecraft has been continued.* Seasonal changes of parameter of thermal inertia of Martian soil have been studied by the statistical method and by the technique of mapping of this parameter for different seasons. In parallel we were being studied trends of the long-term variations of water content in the upper layer of Martian regolith and mapped the normalized fluxes of high-energy neutrons (sounding to the depth of 20–30 cm), acquired for two full Martian years (four terrestrial years). The technique of determination and mapping of the water ice increase in the winter season in the surface layer of Mars at intermediate and high latitudes based on seasonal variations of the parameter of thermal inertia has been worked out. It was shown that spatial variations of the thermal inertia parameter are mostly due to variations of the coefficient of conductivity, while the latter are determined by the content of ice in the surface layer being equivalent to the day skin layer (3–10 cm). Amounts of the winter increase of ice content in the soil have been mapped for three sectors of the planet (70° of longitude) within the ±50° latitudes belt, where the winter covers of CO_2 are absent. It was found that for the 40-50° latitudes of both hemispheres the water ice content increases by 4-10% and in lower latitudes by less than 2 % (Figure 5). The work results have been presented at the 7th International Conference on Mars, Pasadena, CA, USA, July 2007, at the 46th Vernadsky-Brown microsymposim, Moscow, Russia, October 2007, and at the International Conference "European Mars Science and Research", Norvijk, Netherlands, November, 2007.

The work has been done jointly with Institute for Space Research, RAS, and Arizona State University, Tempe, USA.

Mars Express: ESA mission to Mars

2.2. *Photogeologic and topoigraphic analysis of the Mars Express HRSC images and Mars Global Surveyor MOLA altimeter for Reull Vallis area on Mars has been fulfilled.* Results of this study show that the Reull fluvial system consists of four parts with different geologic histories. The lower Reull (jointly with Teviot Vallis) is the most ancient fluvial feature formed from the yet unknown source and serving as a collector of other water flows, which formed other hypsometrically higher parts of Reull. The upper Reull initiated within the lava plateau Hesperia

from the source now buriede under lava covers. Water flows which formed the upper Reull were accumulated in the southern part of the Hesperian plateau and formed there a giant lake (Morpheus basin, the third part of the fluvial system) whose break-up led to formation of the middle Reull (Figure 6). The work results have been published in Journal Geophysical Research.

The work has been done jointly with University of Oulu, Finland.

2.3 *Photogeologic analysis of regions of two the largest volcanoes of Mars, Alba Patera and Olympus Mons, has been fulfilled aiming to decipher their geological histories and to search for connection between volcanic and hydrologic activities in these regions.*

Photogeologic analysis of the surface structure of one of the largest volcanoes of Mars, Alba Patera (D = 1100 km) has been done. It was found that the volcano has a long history of evolution mostly determined by eruptions of non-viscous, probably basaltic lavas. The northern slope of the volcano is cut by narrow channels providing evidence of water erosion in Late-Hesperian - Early-Amazonian time. In the model suggested by us, formation of these channels is due to precipitation of ice from the atmosphere, formation of glacier on the volcano northern slope, and melting the glacier floor probably caused by the increased heat flux in this volcanic area. Analysis of data of the HEND neutron spectrometer shows that in the near-surface layer of Alba Patera the water-containing phases (water, ice, water containing minerals) are absent. This means that these phases, if present, are buried deeper than the depth of sounding by the neutron spectrometer (a few meters).

Photogeologic analysis of structure of the eastern flank of another giant volcano of Mars, Olympus Mons (D = 600 km), has been done. At the foot of the volcano slope has been identified a complex of fluvial channels resembling catastrophic flood valleys formed by release of the artesian water on the surface (Figure 7). The channels are deformed by the compressional deformation and cut by chains of small volcanic domes. From the impact crater density on the floors of these channels it was possible to estimate their age. It was found to be very young: 30–40 m.y. So at the eastern flank of the volcano was found evidence of a complex of very young processes with participation of liquid water, volcanic eruptions and tectonic deformation implying hydrothermal activity at the depth. The latter is especially interesting for searching areas in which at the depth could be environment for existence of primitive forms of life.

The work has been done jointly with Free University of Berlin, Germany, University of Oulu, Finland, and Brown University, Providence, RI, USA.

2.2.4. D.V. SKOBELTSYN SCIENTIFIC-RESEARCH INSTITUTE OF NUCLEAR PHYSICS OF M.V. LOMONOSOV MOSCOW STATE UNIVERSITY

2.2.4.1. Project "GLONASS"

Two successive launching of satellite GLONASS series were realized in 2007 with 6 sets of devices of the control of environment developed and created in SINP MSU. Interesting experimental information was obtained.

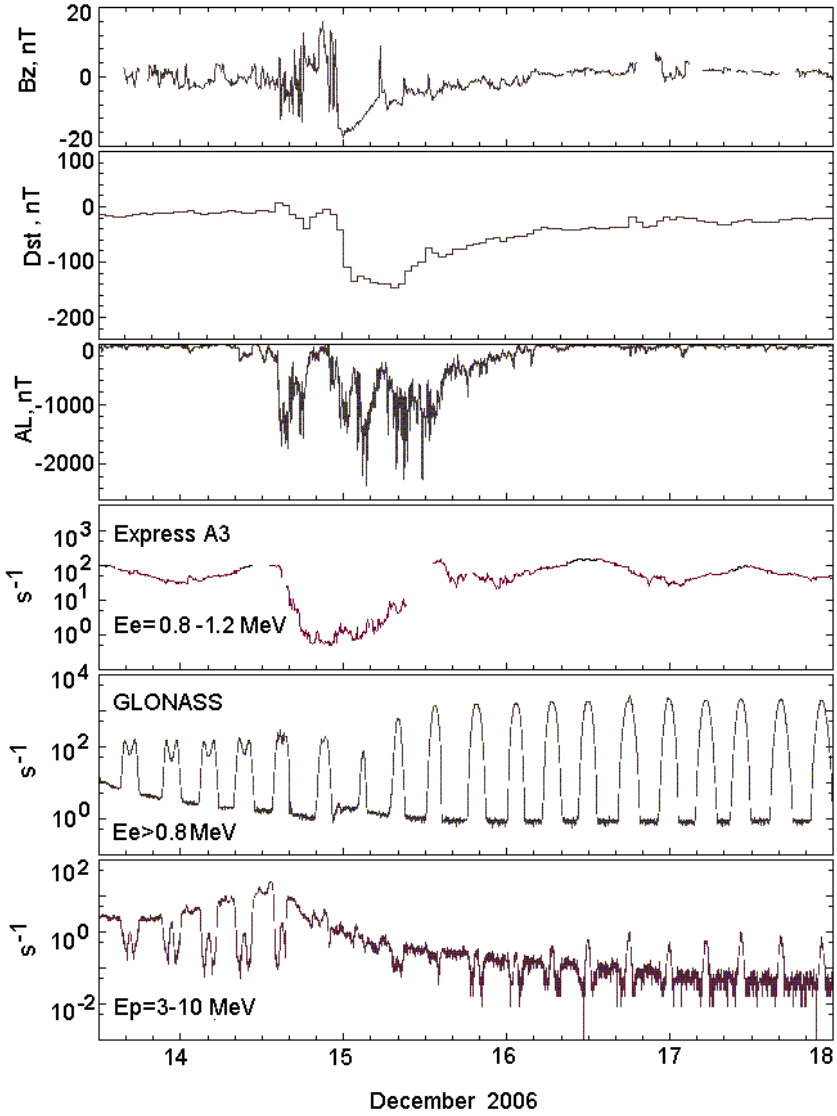

Figure 8: Time dependence of electron fluxes with energy E_e = 0.8–1.2MeV (Express-A3), electrons with energy E_e > 0.8 MeV and protons with energy E_p = 3–10 MeV (GLONASS) for period 13–17 December 2006. Upper part of the figure is B_z component of interplanetary magneticfield (IMF), Dst variation, AL index.

The results of measurements by devices of SINP on satellite GLONASS launched on circular orbit with the inclination ~65° and geostationary satellite Express-A3 give the possibility to obtain the unique information on the dynamics of radiation belt and boundaries of penetration of solar cosmic rays during great magnetic storm 14 December 2006.

Series of powerful solar flares in the December 2006 created great disturbance in the interplanetary space and in the geomagnetic field. Great magnetic storm was developed 14 December (Dst = –146 nT).

Electron fluxes (see Fig. 8) on the boundary of radiation belt (E_e = 0.8–1.2 MeV measured by satellite Express-A3) was decreased on two orders of magnitude. They were restored after storm till prestorm level. However electron fluxes with energy E_e > 0.8 MeV were increased on the order of magnitude in comparison with prestorm level at GLONASS orbit on L ~ 4. Maximum of electron belt (L_{max}) with energy E_e > 0.8 MeV was at L = 4.6. Maximum of the belt displaced in the region L < 4 (L = 4 is the minimal value of L of GLONASS orbit) as the result of storm.

Proton fluxes (see Fig. 9) of radiation belt with energies E_p = 3–10 decreased during main phase of the storm and then nearly reached the prestorm level till the end of the recovery phase.

Solar protons with energies E_p = 3–10 MeV, boundary of which penetration was at L ~ 6.2 in nighttime magnetosphere, fill GLONASS orbit during storm main phase till minimal L~4. Variations near equatorial plane of boundaries of solar proton penetration during specific substorm developed in the moment sudden storm onset were for the first time investigated.

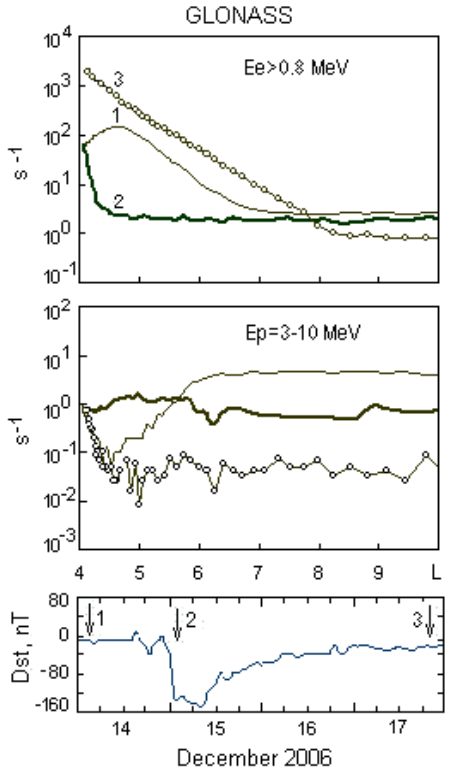

Figure 9: Space distribution of electron fluxes with energy E_e > 0.8 MeV and proton fluxes with energy E_p=3 -10 MeV before storm (curve 1), during main phase of the storm (curve 2) and after storm (curve 3).

2.2.5. INSTITUTE OF COSMOPHYSICS OF THE MOSCOW INSTITUTE FOR ENGINEERING AND PHYSICS

2.2.5.1. International Russian-Italian Mission "RIM-PAMELA" with Participation of German and Swedish Scientists for Investigation of the Fluxes of Antiparticles in Galactic Cosmic Rays

The launch of spacecraft "RESURS DK1" N 1 that has been designed for the photographing of the Earth's surface with high spatial resolution was executed at Baikonur cosmodrome 15 June 2006 (Fig. 1). The satellite was shipped onto an elliptic orbit with perigee 350 km and apogee 600 km. The orbit inclination was 70.4º. The planned life time is three years.

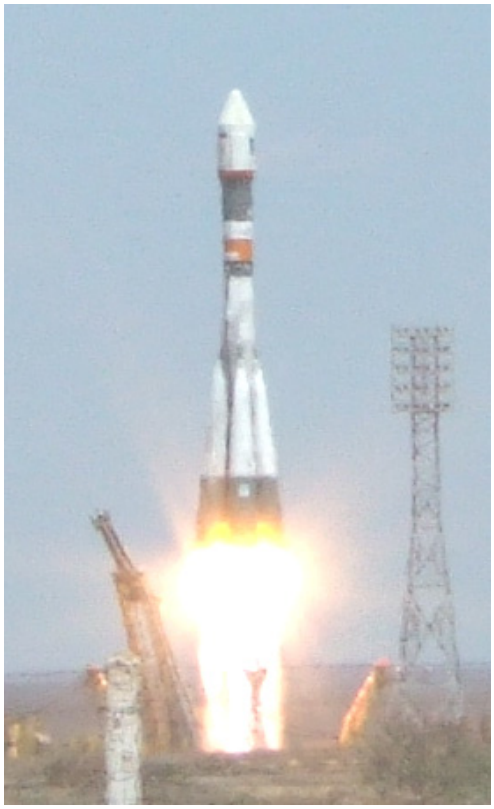

Figure 1: The launch of spacecraft "RESURS DK1" N 1

The precise magnetic spectrometer "PAMELA" was installed within the same spacecraft as an additional scientific load. It has been designed for registration of fluxes of galactic cosmic antiparticles (antiprotons, positrons, antinuclei), electrons and isotopes of light nuclei within the wide energy range from 100 MeV/nucleon up to 200…300 GeV/nucleon (in case of total spectrum of all particles up to 1000 GeV/nusleon).

As the optical system of the satellite is directed most of time on subsatellite point (nadir) and axis of magnetic spectrometer is directed on local zenith (Fig. 2), there is opportunity to realize practically permanent registration of primary cosmic rays fluxes. There is an especially important fact that the measurements are carried out beyond the atmosphere where secondary particles are generated imitating galactic primary fluxes.

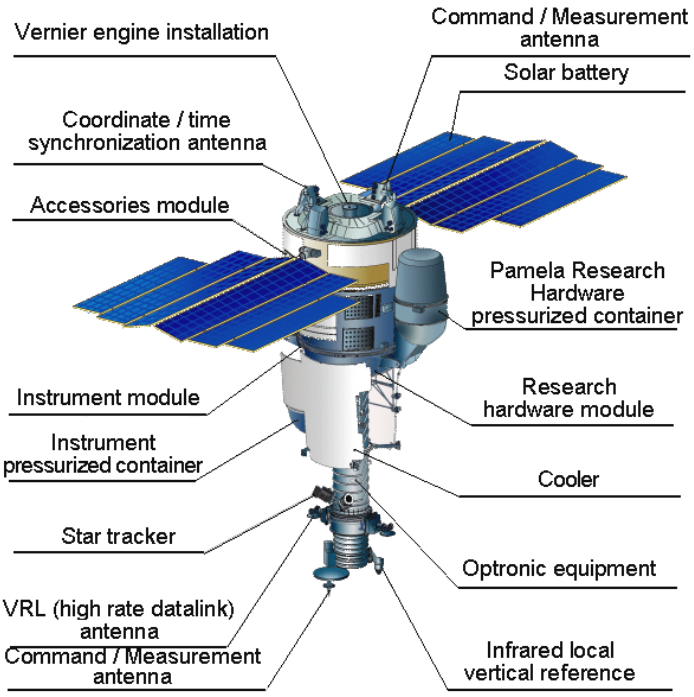

Figure 2: The schematic of placement spectrometer “PAMELA” at spacecraft “RESURS DK1” N 1

The information about intensities and energy spectra of the registered particles is necessary for the solving many problems like:

- the reason of apparent baryonic asymmetry of the Universe;
- the nature of dark matter;
- the physical conditions for generation and spreading of cosmic rays in the Galaxy;
- the peculiarities for solar modulation of primary cosmic radiation different charge signs;
- the generation of isotopes of light nuclei during solar flares;
- the problems of near-Earth space physics and first of all the influence of solar activity on radiation belt of Earth.

Magnetic spectrometer “PAMELA” was developed and created by Italian, Russian, Swedish and German scientists (fig. 3) for realization of program of experiment “a **P**ayload for **A**ntimatter **M**atter **E**xploration and **L**ight-nuclei **A**strophysics”.

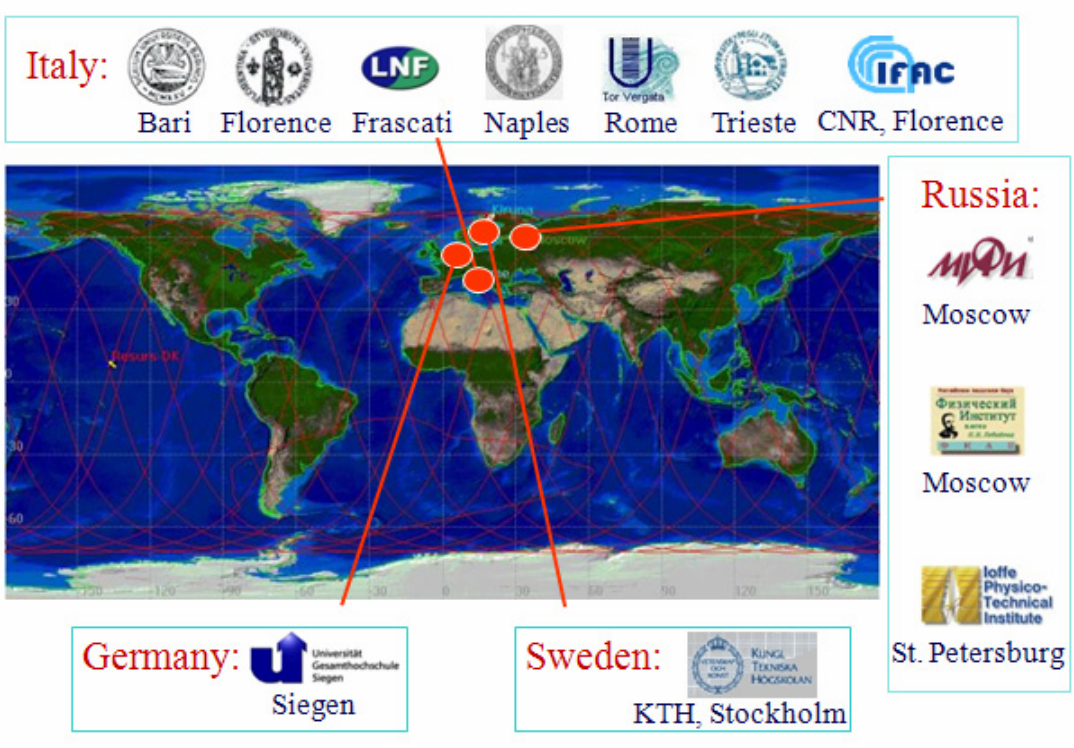

Figure 3: The collaboration “RIM-PAMELA”

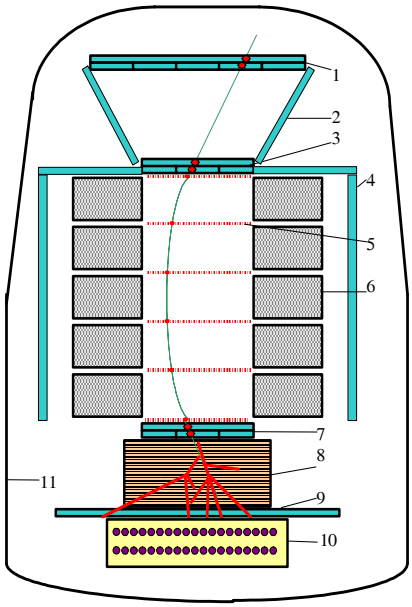

Figure 4: The magnetic spectrometer “PAMELA”. 1, 3, 7 — time of flight system; 2, 4 — anticoincidence system; 5 — silicon strip tracker (6 double plates); 6 — magnet (5 sections); 8 — silicon strip imaging calorimeter; 9 — bottom scintillator S4; 10 — neutron detector; 11 — pressurized container.

The physics scheme of the instrument includes (Fig. 4): the magnetic system for the measuring of the charge sign and particle momentum; the Time of Flight system (ToF) to determine the velocity and arrival direction of particle; the calorimeter to measure the particle energy; the shower detector to measure energy of particles leaving calorimeter; the neutron detector to separate electrons and positrons on proton background; the anticoincidence system to exclude particles that arrived beyond spectrometer aperture; the electronic system for control of the telescope and mass memory of 4 GBytes.

Physically the magnetic system consists of six double silicon strip detectors (tracker) placed into field of five-section constant magnet.

The strip system used allows the measurement of the coordinates of the particle while passing through magnetic field up to several microns (~3,5 mkm). The magnetic field value in center of magnetic system is ~0,48 T where detectors are disposed; the inner sizes of magnetic field are 160×140×450 mm. With these magnetic system performances we can measure momentum of particle up to 700 MeV/c. The precision of momentum measuring within the range of 0.1…300 GeV is about 5 %.

The Time of Flight system consists of three two-laer scintillation counters (S1, S2, S3), each of them consists of separate paddles being observed by photomultipliers from both ends. The Time of Flight system has time resolution $0{,}4 \cdot 10^{-9}$ s, that assures reliable measuring of velocity and direction of particle movement.

The calorimeter consists of 22 tungsten plates with a thickness 0.74 of radiation length, each of them is disposed between 2 silicon strip detectors directed perpendicular to each other with strip width of 2.2 mm. Such a position-sensitive calorimeter allows it to register spatial development of shower generated by through-passing particles interaction with matter of detector; to measure energy of particles of showers; and to distinguish the showers generated by electrons or positrons from showers created by protons and nuclei.

The shower scintillator detector (S4) is placed just under the calorimeter. The sizes of S4 override the sizes of calorimeter low plane. Therefore there is opportunity to detect particles that are emergent from low part of calorimeter and to measure the part of the energy carried away with them. Moreover, S4 can be included in trigger that allows it to register events with high energy deposit inside the calorimeter.

The neutron detector consists of two-layer gas neutron counters filled with $^{3}_{2}\mathrm{He}$ isotope and a three-layer polyethylene moderator. The interactions of electrons and positrons inside the calorimeter are different form interactions of nuclei over shower form as well as large number of neutrons. A large number of neutrons generated for hadron shower are slowed down to thermal energy by polyethylene moderator and then registered by the helium counters. This is one more method for the separation of electrons and positrons on the proton background.

Finally, the system of scintillation counters surrounding the Time of Flight system registers particles passing from sides through detectors during appearance of trigger signal.

Practically all detectors of the instrument allow the measurement of energy lost by a cosmic particle while passing through them. The knowledge of energy losses gives additional information about energy and value of electrical charge of a particle.

The electronic systems of the magnetic spectrometer have satisfied the technical and physical requirements necessary for science equipment onboard of the satellite.

Mode of operation of PAMELA is following: while a cosmic particle is passing through the instrument, i.e. through counters S1, S2 and S3, the trigger signal is produced that gives command to pickup information from all detectors of spectrometer, namely from strips of the tracker, from strips of the calorimeter, from the shower counter S4, from the neutron detector, from the counters of anticoincidence. Then this information is recorded into the spectrometer mass memory. The trigger system is blocked during time of information pickup and its recording into memory of the instrument. The mean size of recorded information within the separate registered event is ~$5 \cdot 10^3$ byte; the dead time being from 2 till 10 milliseconds. The main characteristics of registered particle like sign and value of charge, mass, velocity, momentum and energy those are determined on earth during the processing of the received information.

The properly sized and mass, thermal, technological and flight models of instrument were created during the process of development and creation of the equipment. A total cycle of autonomous tests as well as complex tests inside the spacecraft were carried out, including autonomous tests of instrument systems in accelerator beams. The main physics and technical performances of the spectrometer are presented in table 1.

Table 1

Geometric Factor	21 sm^2sr
Energy range of measurements:	
protons, antiprotons	0.08–200 GeV
electrons, positron	0.05–300 GeV
nuclei, ntinuclei	0.1–200 GeV/nucl
Linear dimensions	90×90×120 sm
Mass	470 kg
Power consumption	355 W

It is significant to note that this is the first time the scientific equipment like the magnetic spectrometer “PAMELA” onboard of this spacecraft has been used which has the capability of the registration of various types of particles with so high energy resolution with the energy range more than three decades. (Fig. 5.)

Figure 5: The photo of flight model of spectrometer “PAMELA”

Figure 6: The Received antenna at NTs OMZ

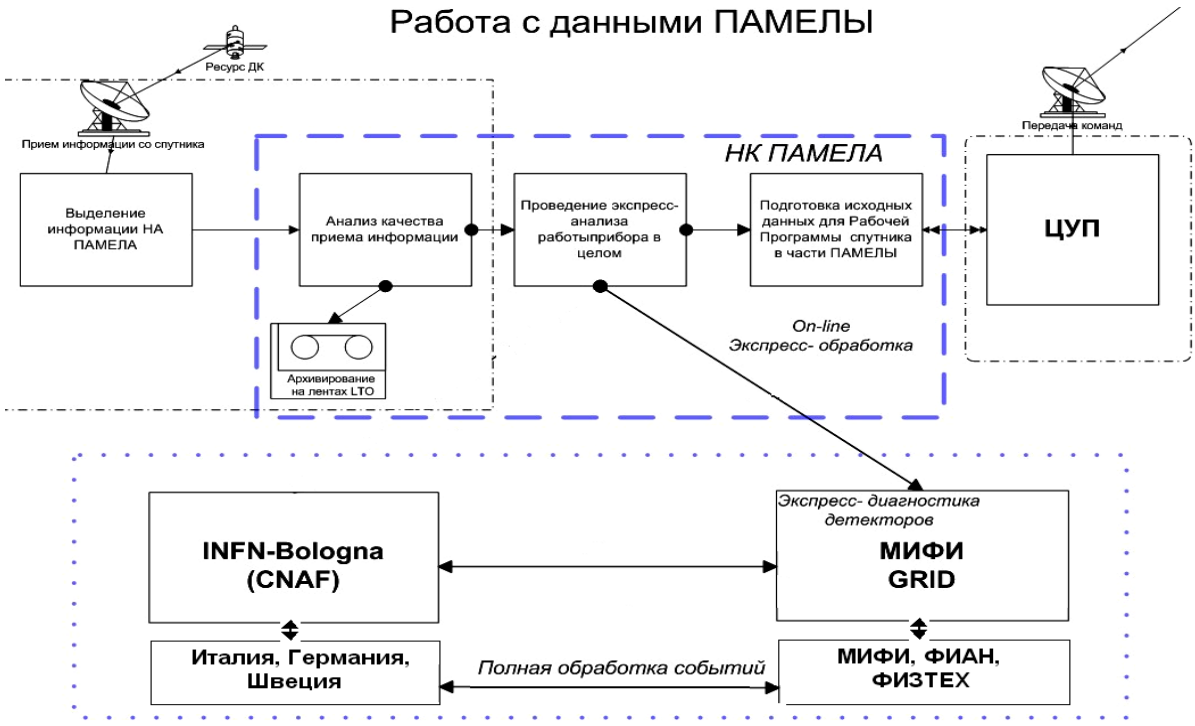

Figure 7: The scheme of information spreading between participants of collaboration “RIM-PAMELA”

During first six months passed after launch of spacecraft “RESURS DK1” N 1 the following order for realization of measuring of fluxes of cosmic rays by magnetic spectrometer was determined.

1) measurements are carried out permanently;
2) the transmission of stored information from memory of spectrometer to the on-board memory is executed once every three hours;
3) the information from spacecraft "RESURS DK1" N 1 is downloaded three to four times per day to the ground receiving station at the Scientific Center of Operational Monitoring of Earth (NTs OMZ) placed in Otradnoe (Moscow) (Fig. 6);
4) the information from spectrometer PAMELA is extracted at the NTs OMZ from the full data stream and delivered to ground segment PAMELA placed at NTs OMZ (Fig. 7);
5) express-analysis of received information is performed at ground segment PAMELA during 30–40 min after each of transmission session with satellite, solutions about the continuation of measurements or necessity to send commands to satellite about changing of routine of spectrometer's work is assumed by the result of express-analysis;
6) in parallel with carrying out of express-analysis "raw" data is delivered to MEPhI (Main organization from Russian side) where the bank of raw data is formed;
7) the scientific information from MEPhI is transferred by using the international scientific net GRID to Russian Ioffe Institute and Lebedev Institute (participants of project) and to the scientific information center of INFN (CNAF, Bologna) where an easy access to this information is provided for all foreign participants of collaboration "PAMELA";
8) the every day work of spectrometer "PAMELA" gives about 14,6 GB of "raw" data. The full volume of raw information at 1 May 2008 is ~ 9 TBytes;
9) the physics treatment and analysis of the obtained results are accomplished by all fellows of "PAMELA" collaboration together.

The physics conditions of the realization of measurements are demonstrated by the following pictures. The counting rate of the appearance of trigger signals (counting rate of instrument) is shown in Fig. 8. One can see in particular this counting rate reaches a maximal possible value of about 100 Hz while the spacecraft is passing through the region of the South Atlantic magnetic anomaly. However, even in that case there is an opportunity for investigation of not only particles trapped in radiation belt, but also galactic particles.

As the orbit of the satellite has big inclination there is opportunity for measurements of fluxes of galactic cosmic particles with minimal energy enough for passing of the three particle counters S1, S2 and S3, signals which form trigger at high geographic latitudes.

Highest energy of the registered particles depends on the light-gathering power of the instrument and observation time. Really the information for antiparticles exists

within the range of 100 MeV up to 100 GeV and for usual particles (electrons, protons and isotopes of light nuclei) exists for energies of 100 MeV up to 350 GeV.

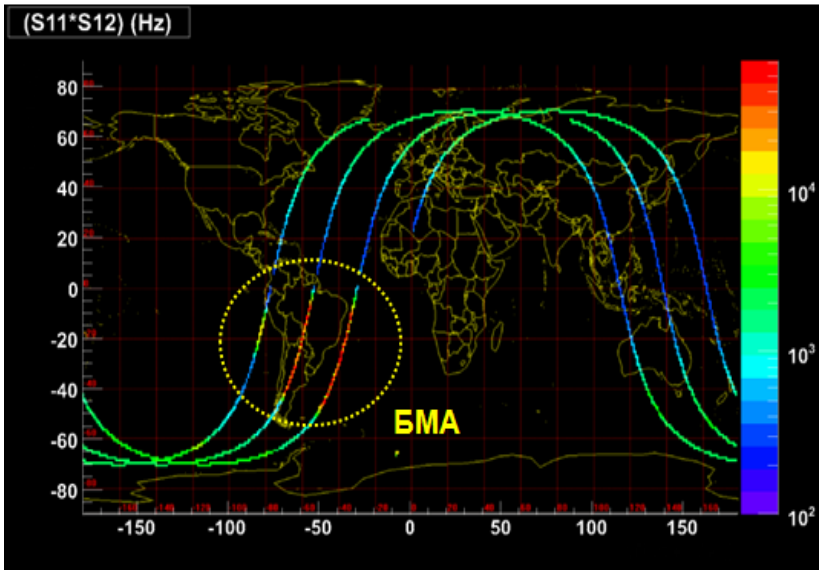

Figure 8a: The counting rate along the orbit of the spacecraft

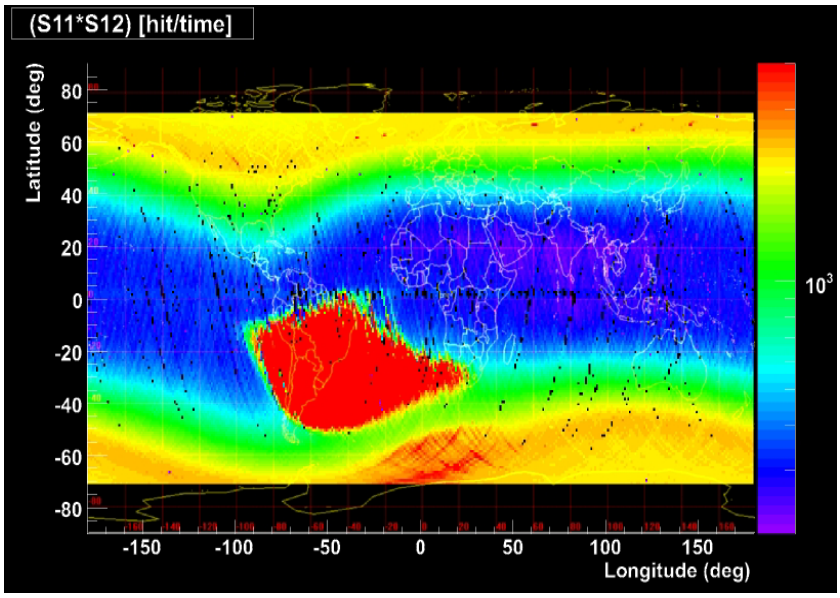

Figure 8b: The general radiation conditions at height of spacecraft

The pictures of passing for various particles (positron, antiproton, proton and nuclear of hydrogen) through the instrument are presented in fig. 9a, 9b, 9c, 9d. Also an example of an event that has appeared beyond the aperture of instrument is shown. Such relative seldom events but with big energy-release in the calorimeter are registered by the instrument as well.

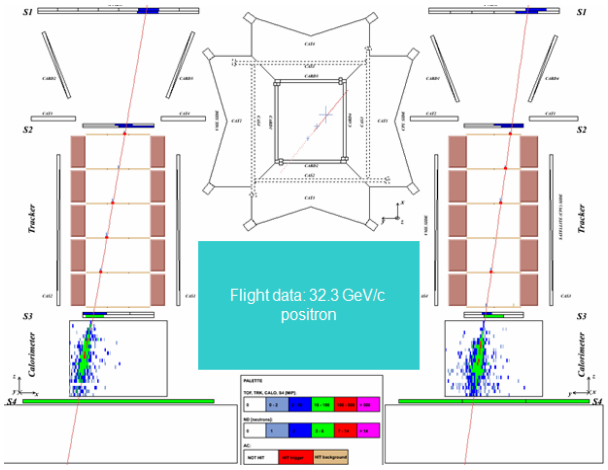

a

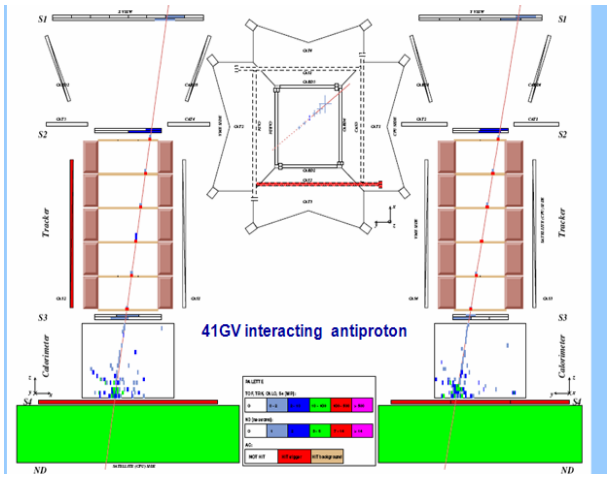

b

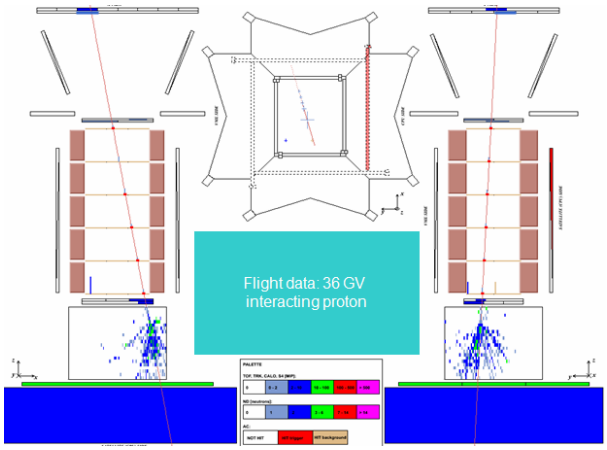

c

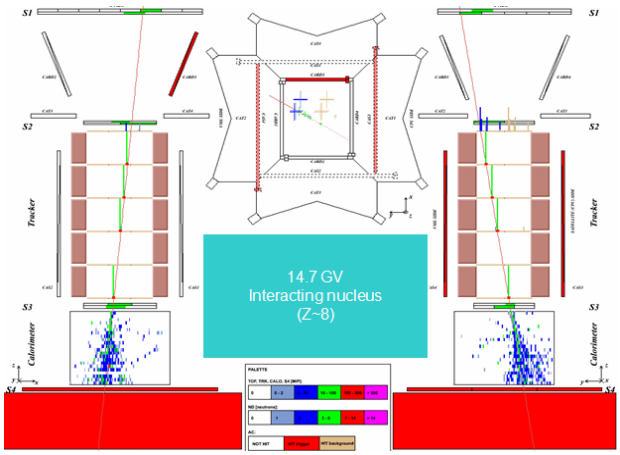

d

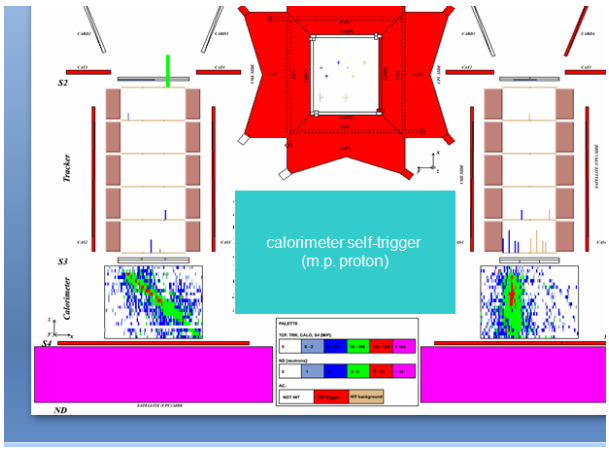

e

Figure 9: The reproduced passing of particles through the instrument: *a* — positron, *b* — antiproton; *c* — proton; *d* — hydrogen nuclear; *e* — flank event. The color of low neutron detector is shown the amount of registered neutrons.

The real opportunities for separation of particles depending on charge are demonstrated in fig. 10a, 10b, where the dependence of energy loss while passing the tracker on their rigidity is presented. Antiprotons and isotopes of light nuclei are enough well distinguished.

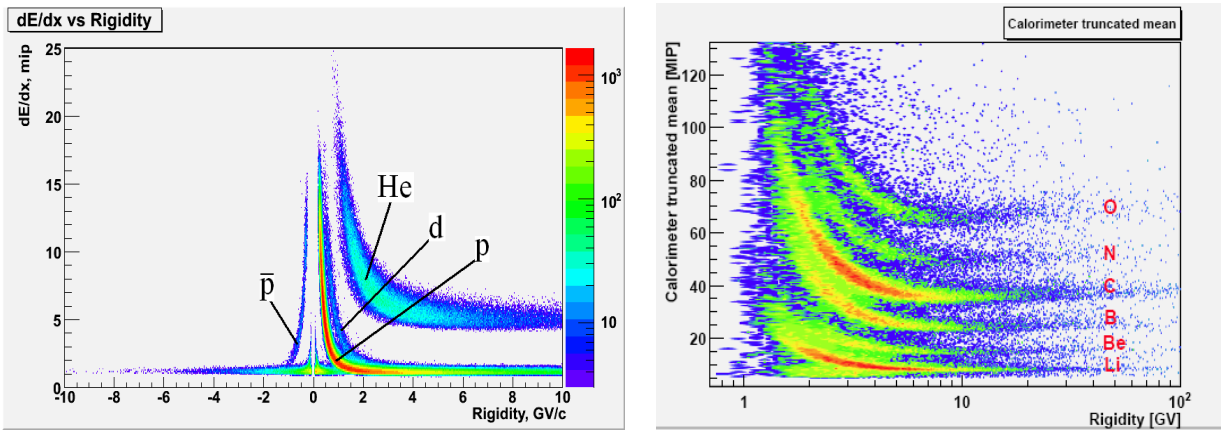

Figure 10: The diagrams: the dependence of energy loss while passing of particles through tracker on their momentum (rigidity).

Some of the preliminary physics results of measurements are presented below.

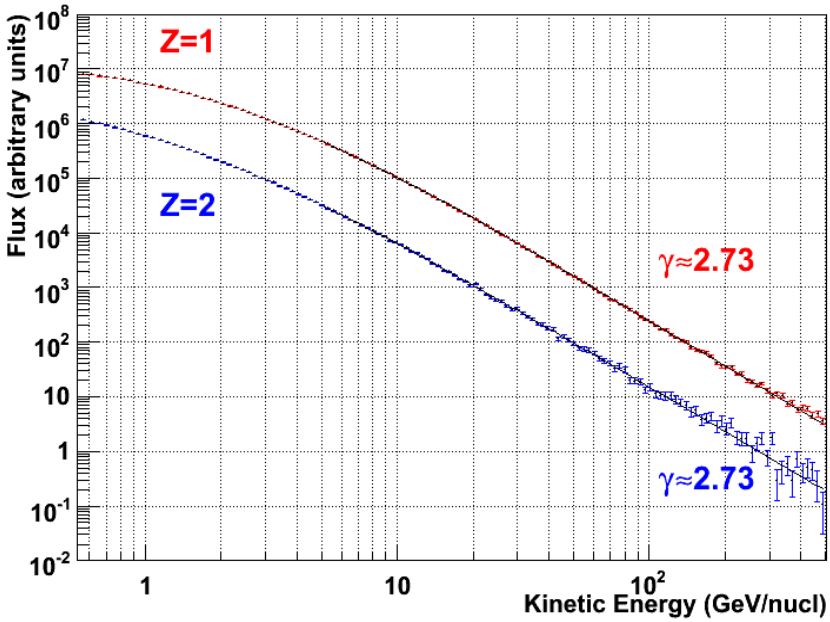

Figure 11

First of all the measurements of energy spectra of protons and helium nuclei. The energy spectra of those particles are presented in Fig. 11. The spectra were constructed by several millions of protons and helium nuclei. The exponents of energy spectra are the most exact values today and similar with precision up to statistic error $\gamma = 2{,}73 \pm 0{,}001$ for protons and helium. This data will be used for more precision mechanisms of acceleration and propagation of particles in the Galaxy. In particular, these results allow for a more accurate calculation of the secondary antiprotons fluxes those are background for antiprotons of annihilation of dark matter particles.

The dependence of the ratio of fluxes antiprotons to protons on particle energy is presented in fig. 12. The contribution of antiprotons from annihilation of particles of dark matter can be found out during this ratio study at high energies.

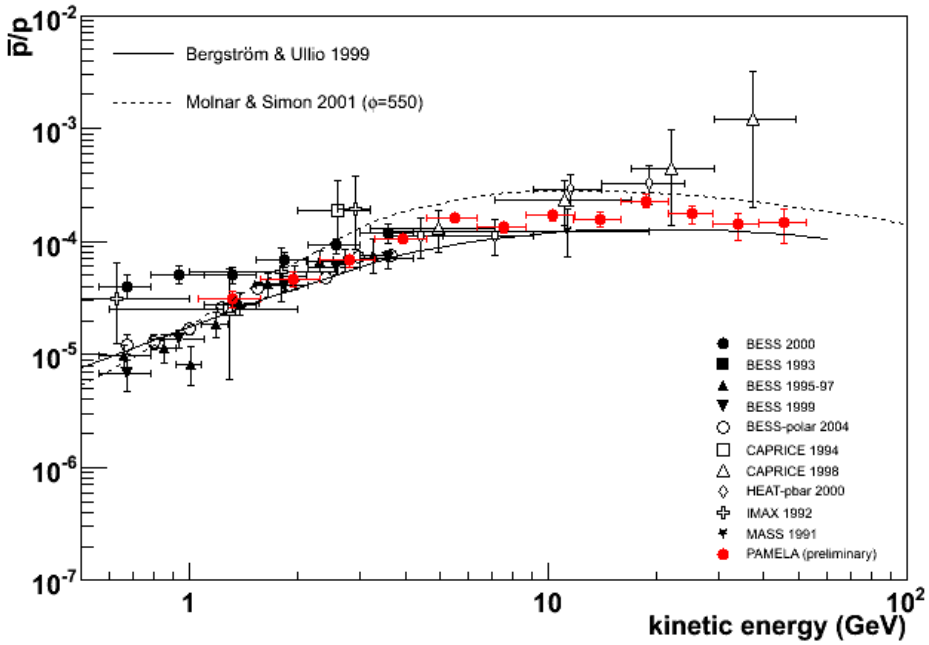

Figure 12: The dependence of ratio of fluxes of antiprotons to protons on energy.

The experimental data obtained in the experiment PAMELA is statistically well-provided and has been obtained within the energies not achieved in other experimental research. And at the same time the data is quite in agreement with calculated values appropriated for secondary nature of antiproton fluxes. Nevertheless just these results are extremely important for construction of theoretical models explaining the origin and properties of dark matter particles.

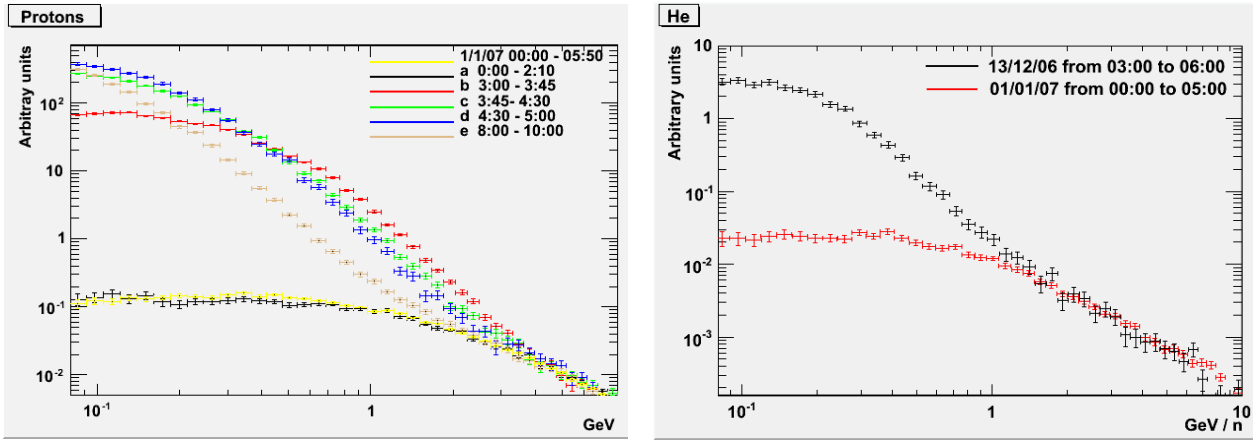

a *b*

Figure 13: The energy distribution of fluxes of solar cosmic rays on energy:
a — protons; *b* — helium.

It is significant to note that the ratio of fluxes of high energy positrons and electrons is a sensitive element for study researching of annihilation of particles of dark matter as well. At this moment the detailed analysis of this ratio is being carried out on the experimental data of magnetic spectrometer "PAMELA". In closure the future results with ratio $e^+/e^+ + e^-$ for different energies up to 100 GeV will be sent to scientific publications.

At the end of 2006 several solar flares were registered in experiment PAMELA. The precision measurements of the fluxes of charged particles with solar origin allowed to obtain the energy spectra of electrons, protons and helium nuclei (Fig. 13).

The flight of satellite "RESURS DK 1" № 1 will be continued at least until the end of 2009. Accordingly the measurements with the unique instrument "PAMELA" will be continued.

2.2.6. IOFFE PHYSICAL-TECHNICAL INSTITUTE OF THE RUSSIAN ACADEMY OF SCIENCES

2.2.6.1. Studies of Cosmic Gamma-Ray Bursts and Soft Gamma Repeaters in KONUS-WIND and KONUS-A Experiments

The nature of cosmic gamma-ray bursts and the mechanism by which giant fluxes of electromagnetic radiation are generated at their sources remain one of the most topical issues of basic space research. In the Russian-American KONUS-WIND experiment, which has been successfully carried out on board NASA's WIND satellite with KONUS Russian scientific instrument since November 1994, a number of new data on the nature of cosmic gamma-ray bursts and soft gamma repeaters has been obtained.

Owing to its high sensitivity, exclusively favorable place of observations in the interplanetary space, and optimal program of observations, the KONUS-WIND experiment is an unique source of information about temporal and spectral characteristics of gamma-ray bursts in the energy range from 20 keV to 10 MeV. These data constitute an essential part of multiwavelength observations of gamma-ray burst sources by spacecraft and a network of terrestrial optical and radio telescopes and are in high demand. The KONUS-A experiment with detectors having a large sensitive surface on board Kosmos-2421 satellite effectively supplemented the KONUS-WIND experiment in 2006-2008.

1. Experimental Procedure

The Russian-American KONUS-WIND experiment, aimed to study cosmic gamma-ray bursts, has been successfully carried out on board NASA's WIND spacecraft since November 1994 with the use of KONUS scientific instruments created by the Ioffe Physico-Technical Institute, Russian Academy of Sciences. The instruments operates under exclusively favorable conditions for observation of gamma-ray bursts. The orbit of the spacecraft lies outside the Earth's magnetosphere, which provides a stable radiation background, absence of interference with the Earth’s radiation belts or shadowing by the Earth, and possibility of uninterrupted observations. The two detectors of the instruments, which are high-sensitivity gamma spectrometers, permanently survey the entire celestial sphere and thereby make it possible to record gamma-ray bursts from any directions. At present, the KONUS-WIND experiment is a unique source of data on the temporal and spectral characteristics of the gamma-ray bursts in the energy range from 20 keV to 10 MeV.

The Russian «Kosmos-2421» spacecraft, which operated in a circumterrestrial orbit from June 2006 till February 2008, carried as an additional payload a set of KONUS-A scientific instruments for study of cosmic gamma-ray bursts. The

KONUS-A experiment was aimed at a comprehensive investigation of characteristics of gamma-ray bursts in observations synchronized with the KONUS-WIND Russian-American experiment. Simultaneous observations of gamma-ray bursts by spectrometric detectors situated at different points in the space and operating in matched measurement modes markedly improve the reliability and validity in recording of fine details of the temporal histories and energy spectra of the bursts. The KONUS-A set of scientific instruments included three spectrometric gamma-ray burst detectors with a large sensitive surface and a record-breaking level of detailedness and informativeness in recording the temporal histories and energy spectra of gamma-ray bursts in a wide energy range from 10 keV to 10 MeV.

The KONUS-WIND and KONUS-A experiments are a highly important source of the most complete data on temporal, spectral, and energy characteristics of cosmic gamma-ray bursts. These data are in high demand by multiwavelength studies of the sources of the bursts, which are carried out at numerous spacecraft and terrestrial radio and optical telescopes owing to the fast and precise localization of the gamma-ray burst sources by NASA's SWIFT mission. The gamma-ray burst detectors also perform a high-sensitivity survey of the celestial sphere in search of exceptional transient phenomena in cosmic X-ray and gamma-ray radiation.

2. KONUS-WIND and KONUS-A Experiments as an Important Component of Multiwavelength Studies of Cosmic Gamma-Ray Bursts

Owing to its wide energy range, optimal program for recording of the principal parameters of gamma-ray bursts, and possibility of surveying the entire celestial sphere, the KONUS-WIND experiment has become an inseparable component of the multiwavelength studies of cosmic gamma-ray bursts, carried out by the extensive network of terrestrial and spaceborne telescopes on the basis of the fast and precise localization of the burst sources by the SWIFT-BAT telescope of NASA's SWIFT mission. Although the detectors of the KONUS-A instruments have a large sensitive surface and provide a noticeably larger value of information, their potentialities are limited by the low circumterrestrial orbit. Nevertheless, their data are of key importance for a number of gamma-ray bursts.

GRB061121. For this bright gamma-ray burst, the spectral evolution of both the “fast” component of the burst and its afterglow were studied in detail because the BAT-SWIFT telescope recorded a burst precursor and, by the beginning of the main phase of the event, the X-ray and optical telescopes of the SWIFT mission were aimed at the burst source. The emission parameters of the source were studied in detail in the range from 1 eV to 1 MeV. The joint observations of the SWIFT and KONUS-WIND instruments yielded an estimate of the isotropic energy flux of the source at $2.8 \cdot 10^{53}$ erg in the energy range from 1 keV to 10 MeV in the rest frame of the burst source. Figure 1 shows results of synchronous observations of the light curve of the source, according to the data furnished by SWIFT and KONUS-WIND instruments, including those obtained in the

background mode by the KONUS-WIND instrument, which independently confirmed the recording of the precursor of the gamma-ray burst. Figures 2a and 2b compare the temporal profiles of this burst, obtained in KONUS-A and KONUS-WIND experiments. The spectral data from the KONUS-WIND experiment were used to find the peak energy and the shape of the energy spectrum for various phases of the burst.

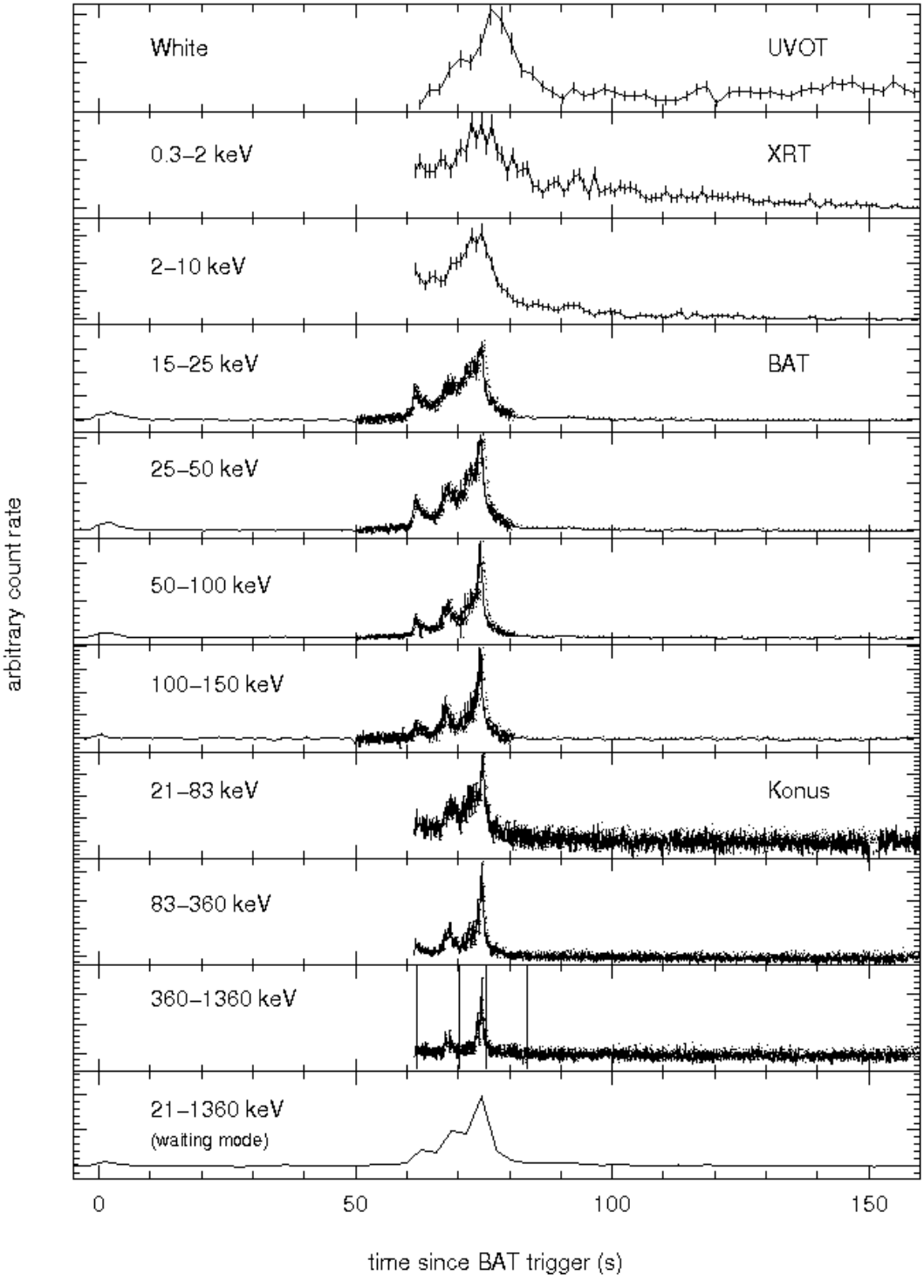

Figure 1: Light curves of the GRB061121.

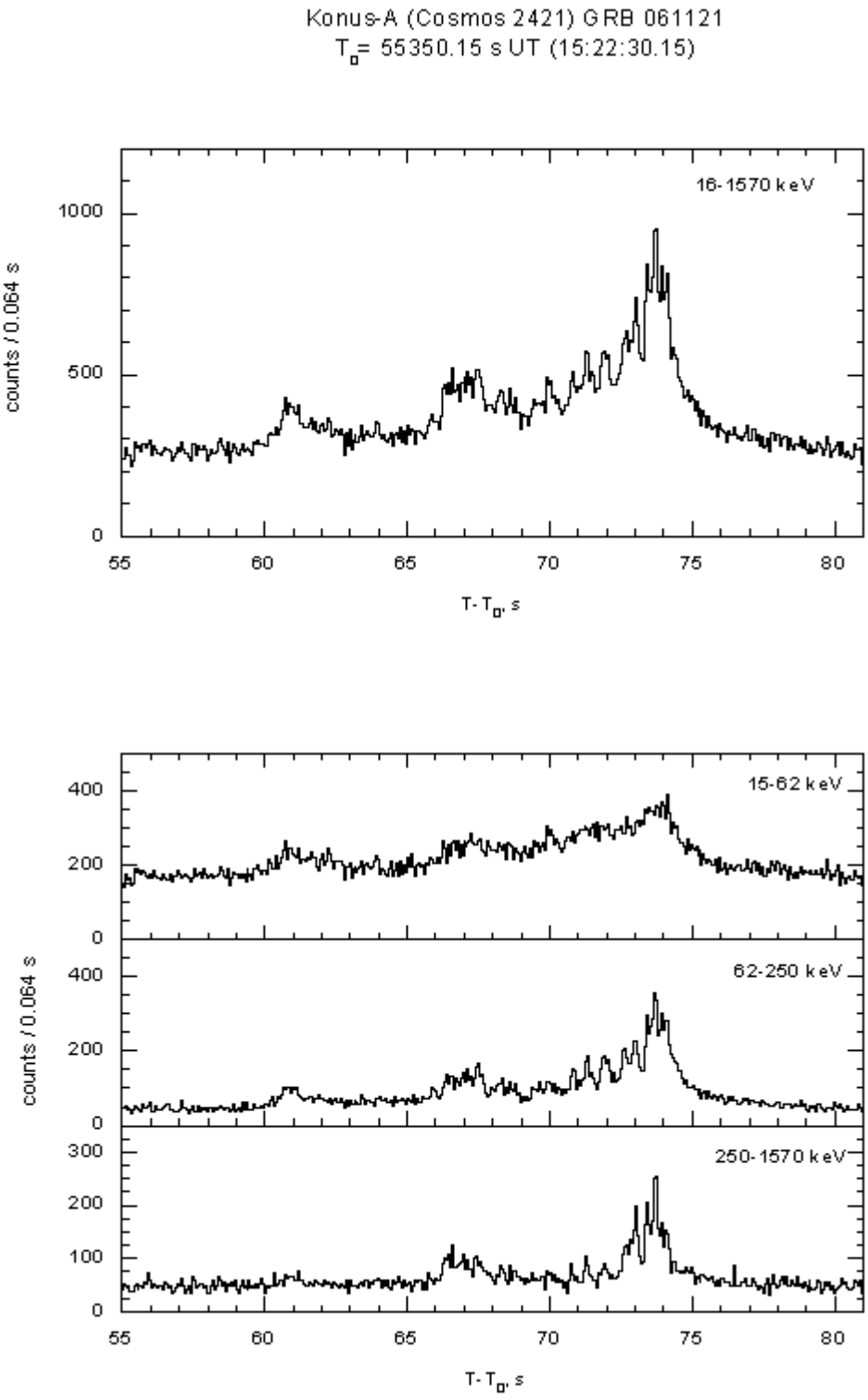

Figure 2a: Light curves of the GRB061121 gamma-ray burst according to the results of the KONUS-A experiments.

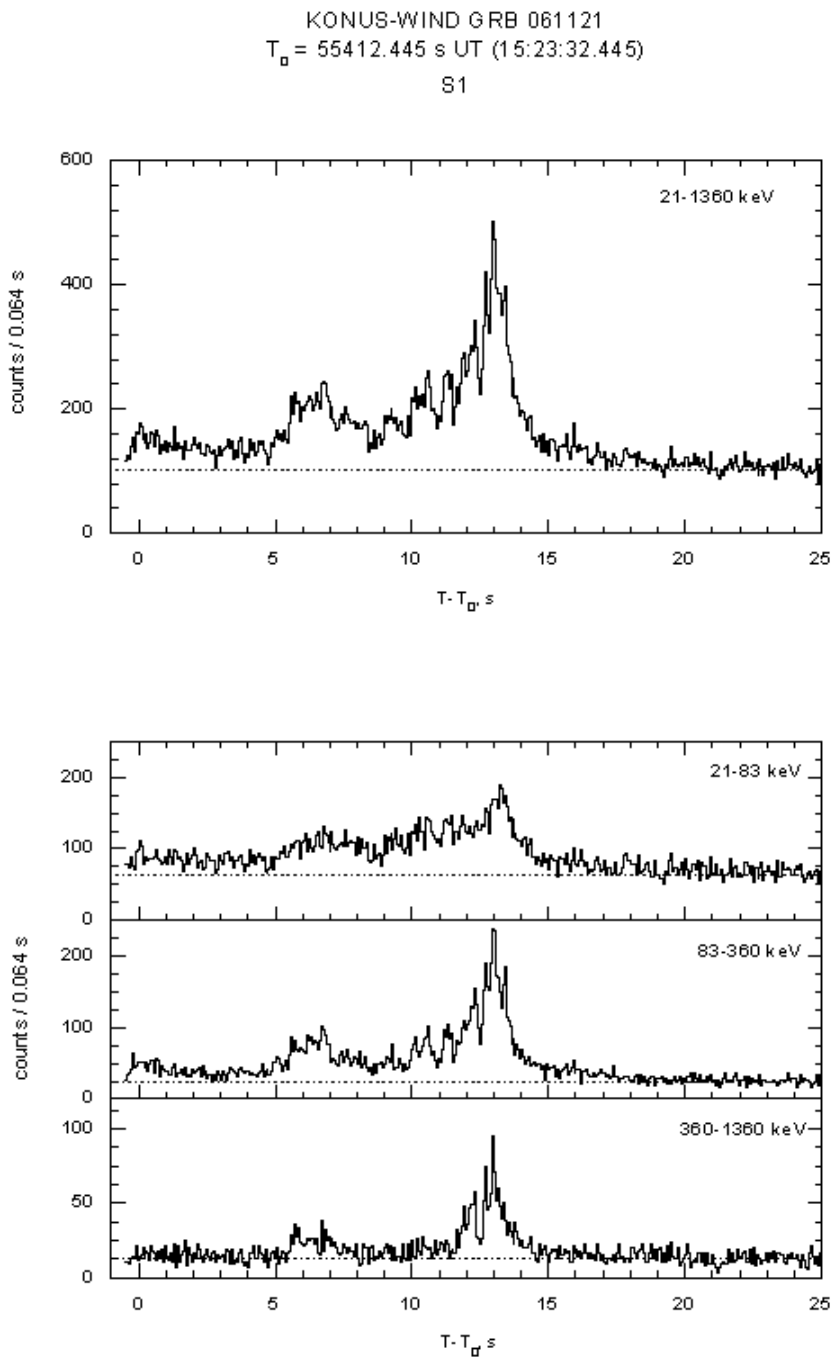

Figure 2b: Light curves of the GRB061121 gamma-ray burst according to the results of the KONUS-WIND experiments.

GRB050713A. Joint observations by the SWIFT mission, KONUS-WIND instruments, XMM-Newton X-ray telescope, and MAGIC terrestrial telescope, which records flashes of Cherenkov radiation from ultra high-energy gamma rays, made it possible to unprecedented coverage for this gamma-ray burst radiation in a wide energy range from 0.002 keV to 500 GeV. Figure 3 shows temporal profiles of the event according to KONUS-WIND and BAT-SWIFT data, and Fig. 4 presents the results of joint fitting of the energy spectra of radiation for this gamma-ray burst.

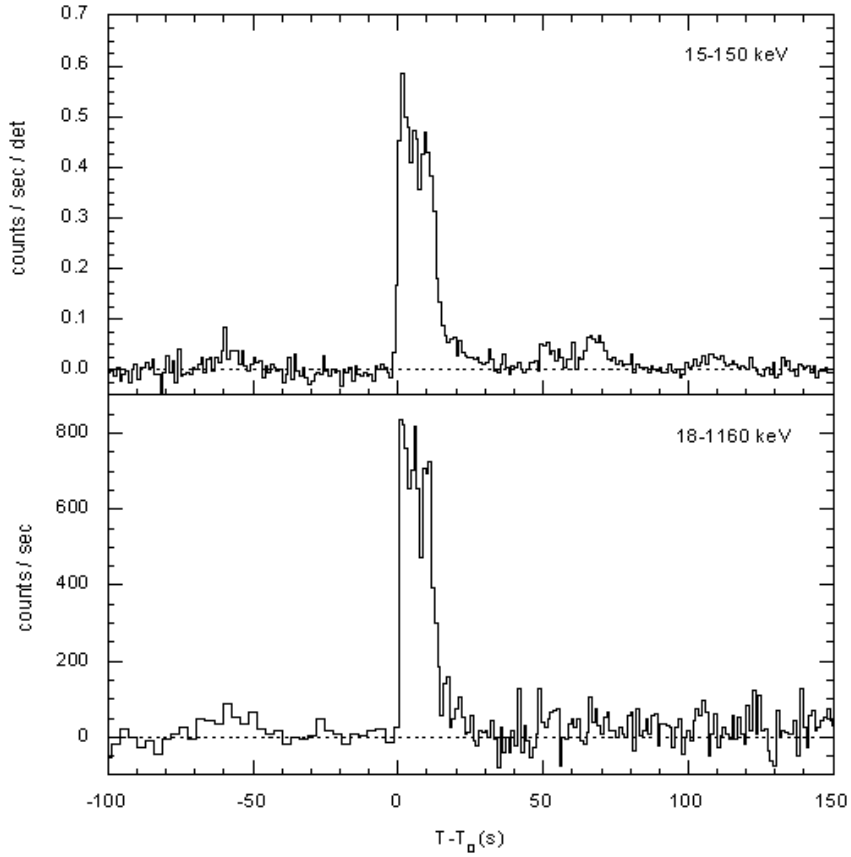

Figure 3: Light curves of the GRB050713A gamma-ray burst according to the data furnished by the BAT-SWIFT telescope (upper panel) and KONUS-WIND apparatus (lower panel).

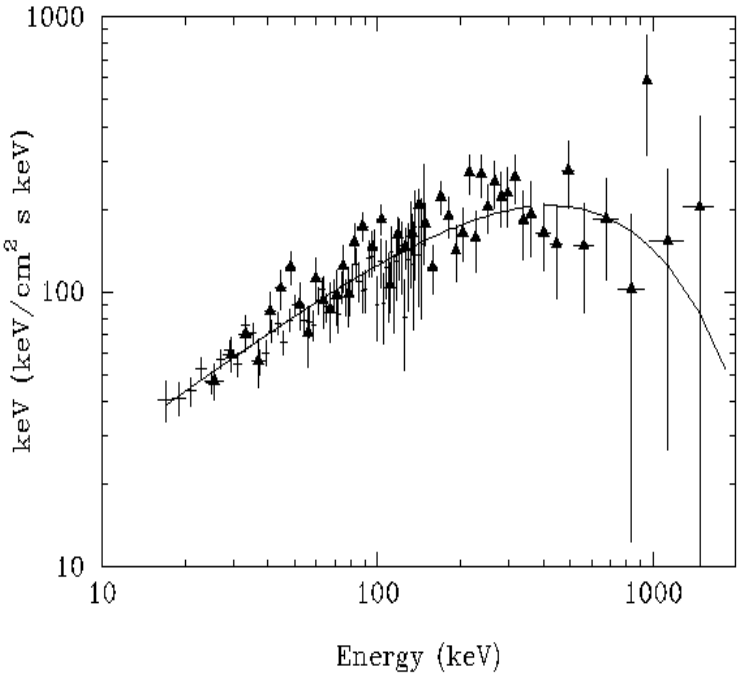

Figure 4: Results of a joint spectral analysis of the emission from GRB050713A, based on the data furnished by the BAT-SWIFT telescope (crosses) and KONUS-WIND apparatus (triangles).

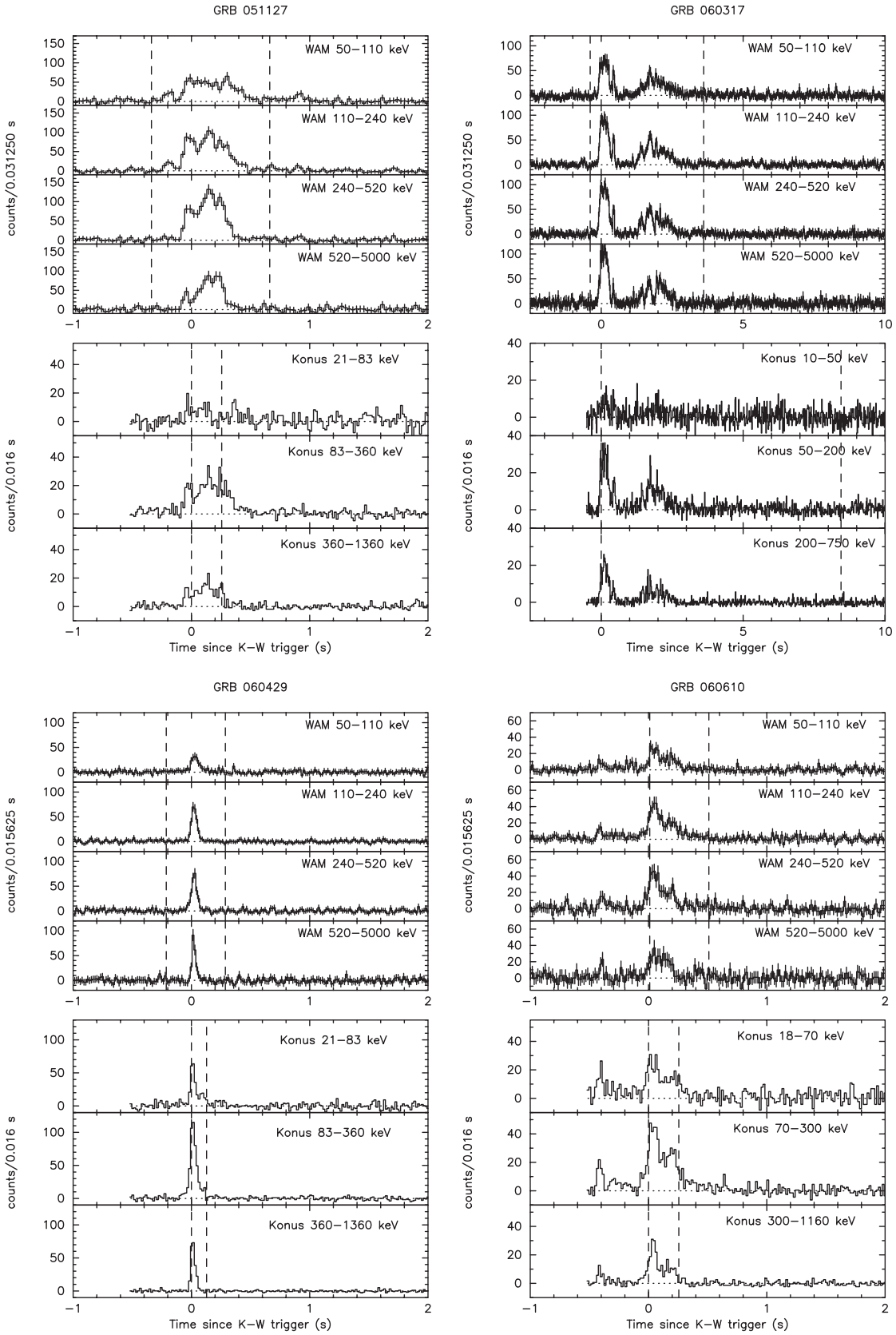

Figure 5: Light curves of two short bursts GRB051127 and GRB060429, plotted using the results of the KONUS-WIND and Suzaku-WAM experiment.

GRB051127 and **GRB060429.** Synchronous observations of these two short gamma-ray bursts were made by KONUS-WIND and Suzaku-WAM instruments. A joint spectral analysis made it possible to study the spectral properties of the bursts in a wide energy range with high precision. It was found that both bursts had a high maximum energy E_p of about 1 MeV and their spectra were described by a power law, which is typical for long bursts. Figures 5 and 6 show light curves for both the events and the results of a joint fitting of the spectral data.

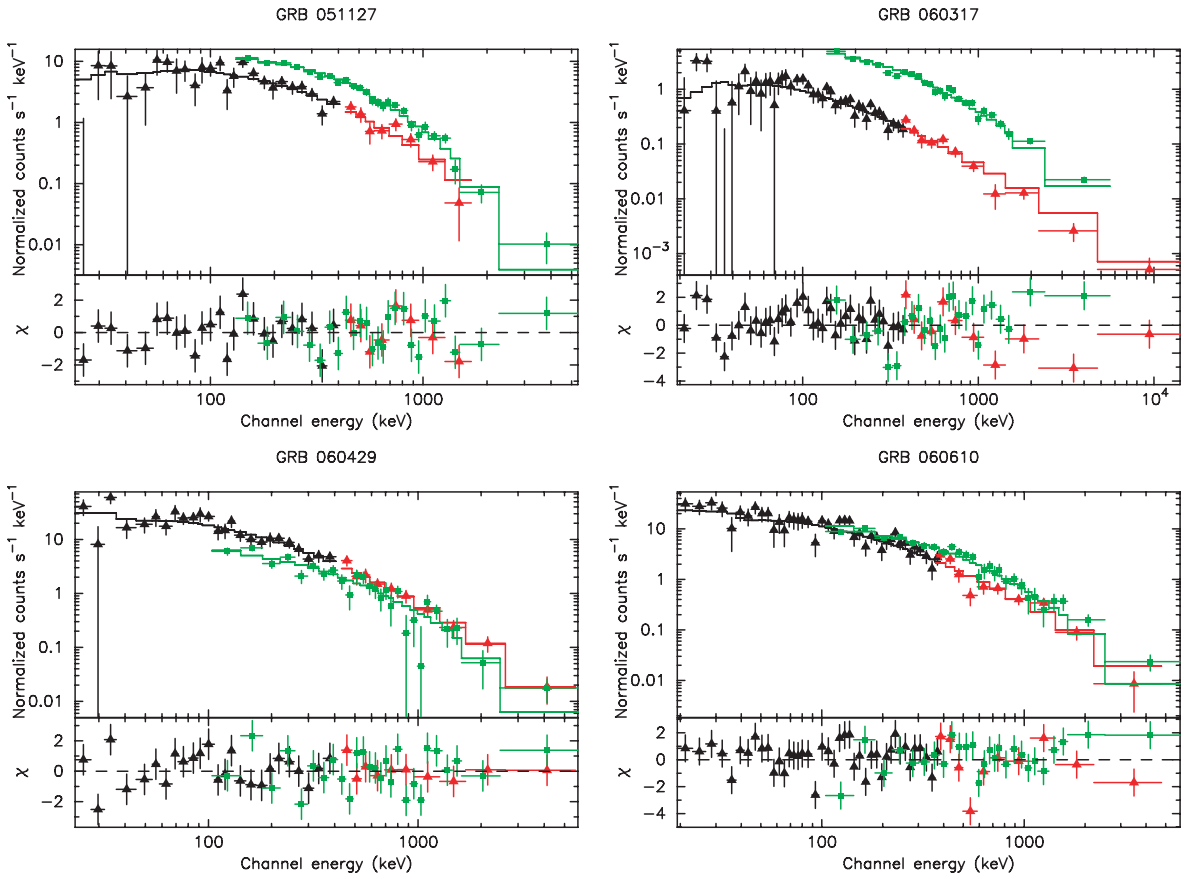

Figure 6: Joint spectral analysis of two short bursts GRB051127 and GRB060429, based on the observations in the KONUS-WIND and Suzaku-WAM experiments.

3. Studies of Soft Gamma Repeaters

In 2007, an additional convincing evidence was obtained that part of the observed short bursts with a hard energy spectrum may be giant flares from gamma repeaters in neighboring galaxies. The first indication of this kind was obtained for GRB051103 as a giant burst in the close group of interacting galaxies, M81. On February 1, 2007, the KONUS-WIND instrument recorded an exceedingly strong short burst with a hard energy spectrum (Fig. 7). The source of the burst was localized by the triangulation method using the data furnished by KONUS-WIND, INTEGRAL (SPI-ACS), and neutron-gamma-ray detector of NASA's MESSENGER mission. The center of the localization box was situated at a

distance of 1 degree of arc from the center of a nearby galaxy, Andromeda Nebula (M31) (Fig. 8). On the assumption that the burst source lies in M31 galaxy at a distance of 0.78 Mpc, the measured flux and the maximum luminosity were $1.5 \cdot 10^{45}$ erg and $1.2 \cdot 10^{47}$ erg·s^{-1}. These values are in good agreement with the corresponding parameters of giant flares observed from other gamma repeaters.

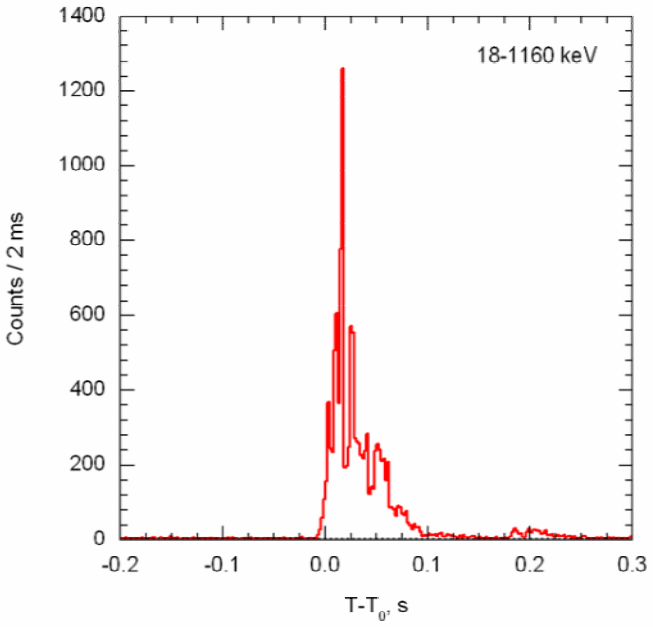

Figure 7: Light curve of the GRB070201 gamma-ray burst in the energy range 17–1130 keV.

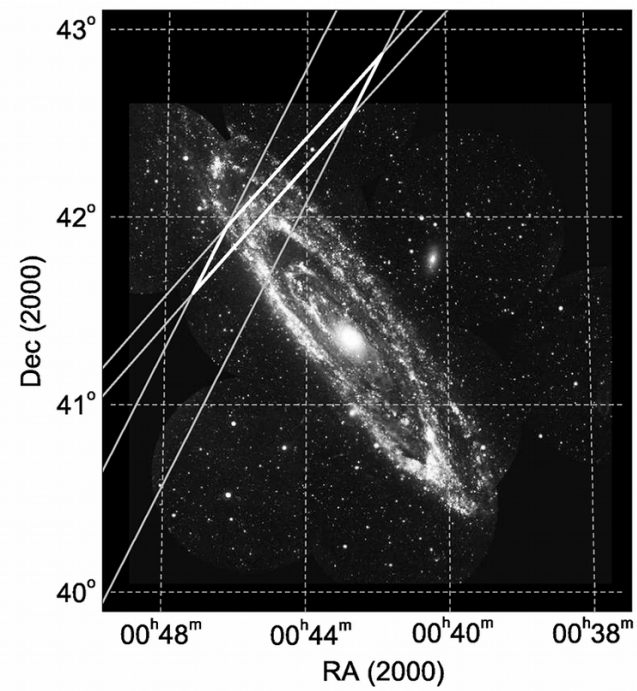

Figure 8: UV image of M31 galaxy and the localization region of the gamma repeater.

A new manifestation of the activity of the SGR1806-20 gamma repeater was studied in July and August 2006 in synchronous observations by KONUS-WIND and KONUS-A detectors. A total of 20 repeated bursts was recorded and studied in detail. An advantage of the KONUS-WIND instrument situated in the interplanetary space was that it enabled a permanent observation of the source. The three spectrometric detectors of the KONUS-A instruments have a substantially larger sensitive surface and provide a record-breaking, as regards the detailedness and informativeness, recording of temporal and spectral characteristics of the bursts. The most interesting in its structure was the event on August 6, 2006. It was a kind of cluster of six separate repeated bursts, the last of which exhibited a periodic structure similar to that observed in the tail of the giant flare from this gamma repeater on December 27, 2004. An analogue of the event on August 6 was earlier recorded by the KONUS-WIND instrument on December 3, 2005. The temporal profiles of these events are shown in Fig. 9.

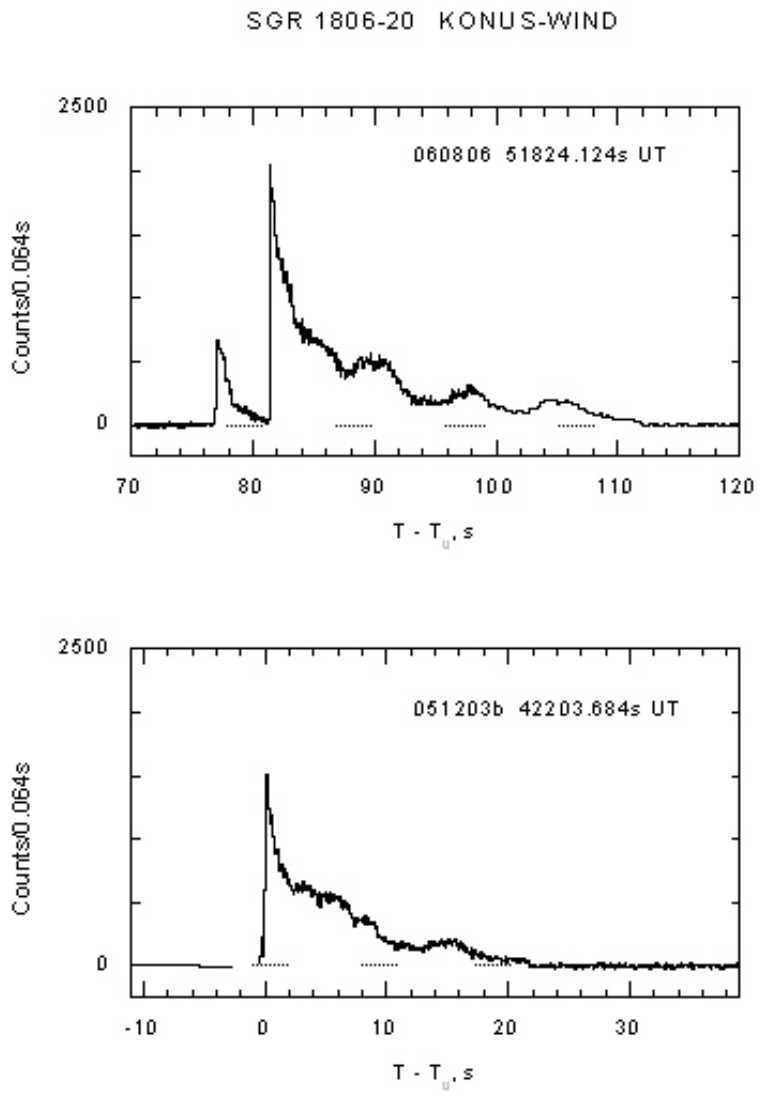

Figure 9: Light curves of soft repeated bursts from SGR1806-20 on August 6, 2006, (upper panel) and December 3, 2005 (lower panel).

One more manifestation of the activity of the SGR1806-20 gamma repeater was studied in synchronous observations of KONUS-WIND, KONUS-A, BAT-SWIFT, Super-AGILE, IBIS, SPI-ACS (INTEGRAL), and Suzaki-WAM instruments in September 2007. An intense burst from this repeater was recorded by the KONUS-WIND instrument on September 7, 2007 (Fig. 10). A total of 18 repeated bursts were recorded on September 14–23, 2007. The data obtained are important for construction of models of this class of relativistic cosmic objects that rarely exhibit their activity.

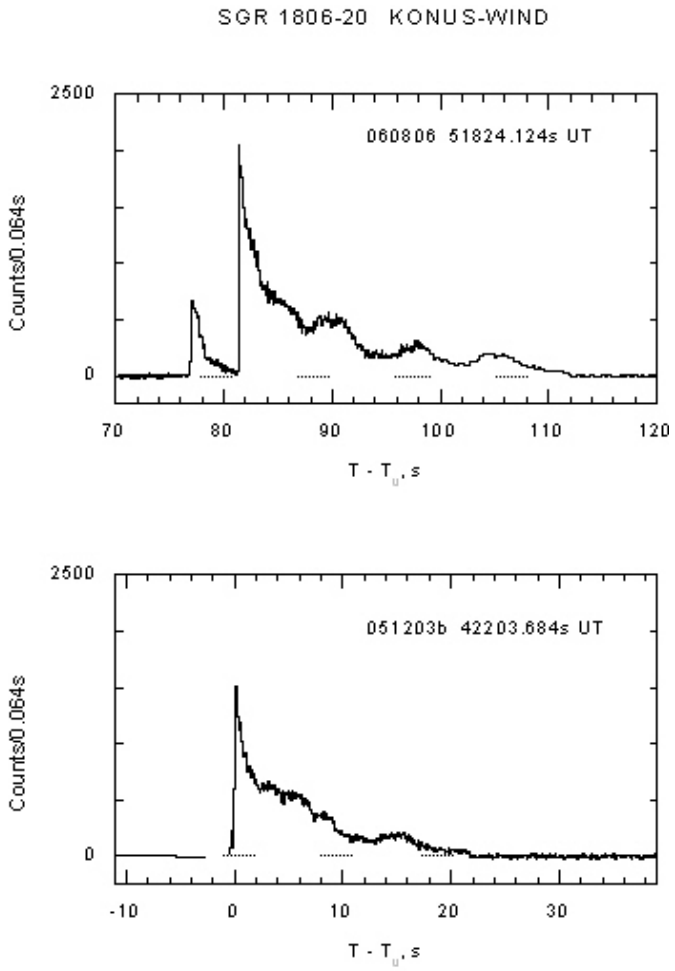

Figure 10: Light curve of the repeated gamma-ray burst from SGR1806-20 on September 7, 2007

4. Observations of Exceptional Transient Phenomena in Cosmic X-ray and Gamma Radiation

The high-sensitivity gamma-spectrometers performing a long uninterrupted monitoring of cosmic gamma-ray bursts also enable to study of exceptional transient phenomena in the cosmic X-ray and gamma radiation, which fall outside the field of vision of narrow-beam telescopes. As an example of such observations can serve studies of the exceptional flare activity of the known Cygnus X-1 X-ray

source in the energy range 20–200 keV by the KONUS-WIND instrument and IPN (Interplanetary Network) instruments in 1996–2002. A new intense flare from the Cygnus X-1 source was recorded on August 7–8, 2007, by the detectors of KONUS-WIND and Suzaki-WAM. It was the strongest burst from this source, with a fluence of $8.0 \cdot 10^{-4}$ erg cm^{-2}. The temporal profile of this event, according to the data obtained in the KONUS-WIND experiment, is shown in Fig. 11.

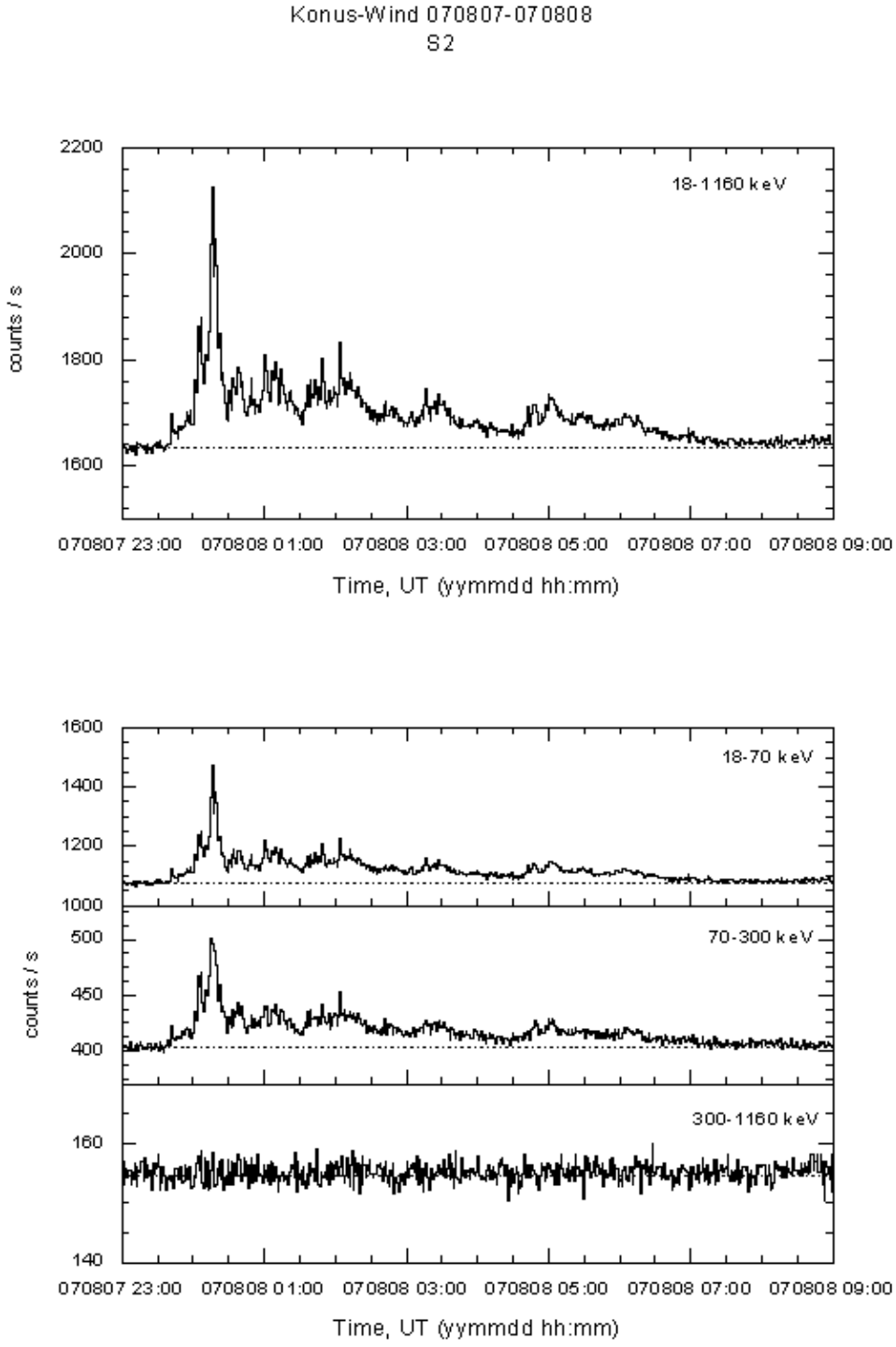

Figure 11: Gamma-ray flare from the Cygnus X-1 source, recorded in the KONUS-WIND experiment on September 28, 2006

A similar, but with a softer spectrum, flare, the so-called super-flare, was recorded by the KONUS-WIND instrument and BAT and XRT telescopes of the SWIFT mission from the EV Lac star on April 25, 2008 (Fig. 12). The flare activity in the spectral range of hard X-ray radiation from this stellar object has also been recorded earlier, but the new flare substantially exceeds in intensity those observed previously. The new data enable to study of the energy spectrum of the flare from the EV Lac stellar object in a wider energy range, from 0.8 to 70 keV.

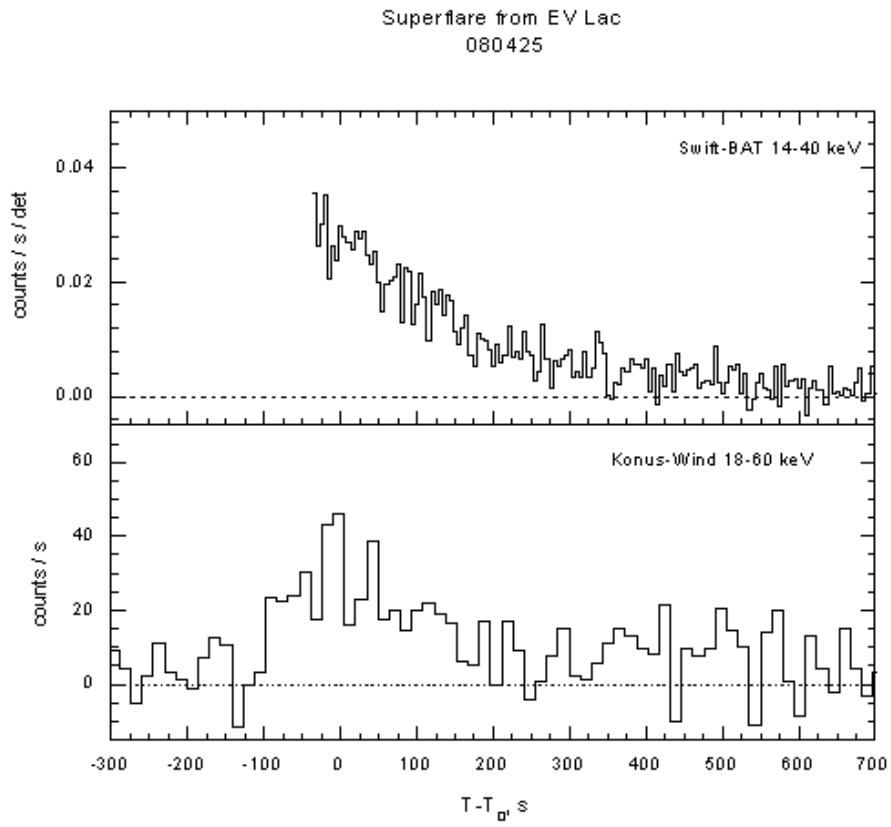

Figure 12: Light curve of the super-flare recorded by the KONUS-WIND instrument and BAT and XRT telescopes of the SWIFT mission from the EV Lac star on April 25, 2008

5. Conclusion

The KONUS-WIND experiment and the synchronized KONUS-A experiment yielded new priority data on the nature of cosmic gamma-ray bursts and a particular rare class of repeating spectrally soft bursts from gamma repeaters. A convincing evidence was obtained that part of the observed short burst with a hard energy spectrum may be giant flares from gamma repeaters in nearby galaxies. Owing to the high sensitivity of the KONUS-WIND instrument in a wide energy range and the optimal conditional of observations in the interplanetary space, the experimental data are in high demand by present-day multiwavelength studies of gamma-ray bursts sources.